STUDY OF PLASMA AND ENERGETIC ELECTRON ENVIRONMENT AND EFFECTS

ESTEC contract 11974/96/NL/JG(SC)

TECHNICAL NOTE, WP120

ANALYSIS OF FREJA CHARGING EVENTS:

MODELLING OF FREJA OBSERVATIONS BY SPACECRAFT CHARGING CODES

SPEE-WP120-TN

Version 2.0

December 21, 1998

Prepared by

Anders I. Eriksson[1], Lars Wedin[1,2], Jan-Erik Wahlund[1], Bengt Holback[1]

[1]*Swedish Institute of Space Physics, Uppsala Division*

[2] *Space Environments and Effects Analysis Section (TOS-EMA), ESA/ESTEC*

ESA Technical Officer: A. Hilgers, Space Environments and Effects Analysis Section (TOS-EMA)

ESA Technological Research Programme, Space Environments and Effects Major Axis

Contents

1. INTRODUCTION

1.1 Scope of document

This document presents the results provided by work package WP120 of the spacecraft charging study made at the Uppsala Division of the Swedish Institute of Space Physics under contract from ESTEC 1996-1998. The central part of this work package is the comparison of five Freja charging events, all included in the WP130 database and presented in WP110, to charging simulations using the POLAR code [c.f. Hilgers, 1994]. This document was written with the following purposes:

- Give a brief introduction to spacecraft charging models
- Give a materials list of the Freja spacecraft
- Present Freja models for POLAR simulations
- Present environment models for POLAR simulations
- Present results of direct POLAR simulations using the above
- List input files for POLAR simulations
- Discuss the simulation results
- Suggest further investigations
- Suggest code development

The presented input files for POLAR simulations are extensively commented in order to facilitate their future use. These files have also been delivered to ESTEC in digital format.

1.2 Disposition

As explained in WP110 and WP130, the Freja instrumentation makes it possible to experimentally study the charging of the whole spacecraft, and this is what is modelled here. Differential charging as such is not a chief consideration in this work as no observational Freja input exists, but some effects of local electrostatic perturbations are investigated.

From the detailed data analysis of WP110 and the statistical survey of WP130 it is clear that spacecraft potential levels below the expected floating potential, as based on the thermal plasma characteristics, often are observed on Freja passes through the auroral zone. It was also shown in these work packages that the spacecraft potential in these cases is closely correlated to electron precipitation above some keV. In WP120, which is presented in the present section, we attempt to model these results using the numerical codes SUCHGR and POLAR, presented in Section 2 together with a brief introduction to some of the basic

physics of spacecraft charging. NASCAP was used in some preliminary work on this study [Svensson, 1996]. Our approach in simulation and modelling is that of an "unprejudiced best-effort": we first describe and model the spacecraft and its surface materials (Section 3), then model its environment (Section 4) as accurately as possible, and finally use this as input to POLAR, the code developed to deal with auroral charging phenomena in low-Earth orbit. We also present results from simulations using variations of the environmental and material parameters used in the modelling. For the simulations (Section 5), we use POLAR version 1.3.7. We find that POLAR used by us in this way does not reproduce the observed charging levels, although variation of material or simulation parameters sometimes get us close to observed voltages. Possible reasons for the discrepancies are discussed. We conclude this study with a summary and recommendations for further investigations and software development in Section 6.

1.3 Related documents

Work package WP100 (Analysis of Freja charging events) is presented in the following documents:

- SPEE-WP110-TN: Charging events identification and case study of a subset of them. Referred to as WP110.
- SPEE-WP120-TN: Modelling of Freja observations by spacecraft charging codes (this document).
- SPEE-WP130-TN: Statistical occurrence of charging events. Referred to as WP130.

WP100 is also presented in Chapter 4 of the SPEE final report, which in addition contains information on the other work packages in the SPEE contract.

2. MODELLING SPACECRAFT CHARGING

There exist a huge literature on the subject of spacecraft-plasma interaction, and we do not intend to review it here. For good introductions to the subject in general, see the recent textbooks by Tribble [1995] or, more detailed, Hastings and Garrett [1996]. Hastings [1995] gives a review of the processes particularly important at low Earth orbit. The published literature also includes several numerical studies of spacecraft charging using NASCAP [e.g. Frezet et al., 1989] or POLAR [e.g. Katz et al., 1989]. Here we intend just to point at some fundamentals important for the understanding of the Freja charging events, particularly how they are modelled by the POLAR charging code.

2.1 Spacecraft Charging Codes

Several software tools for modelling spacecraft surface charging exist. Most well known and commercially available is the NASA Charging and Analysis Program, NASCAP, developed in the USA in 1980s. The original version of NASCAP, also known as NASCAP-GEO, was intended for simulation of geostationary orbit conditions, but a version NASCAP-LEO for low Earth orbits has also been developed. For the study of charging effects on satellites in polar orbits, the code POLAR was developed from NASCAP in the late eighties. POLAR has additional capabilities to model auroral electron precipitation, which is the essential source of spacecraft charging on polar orbits. In Russia, the ECO-M and COULOMB codes have been constructed and used [e.g. Danilov et al., 1998; Krupnikov et al., 1992]. These codes, which are not considered in the present work, are reported to be similar to NASCAP in scope but with extended capabilities for modelling of radiation induced discharges for the 12 hour Molniya orbits [Hastings and Garrett, 1996]. Common to these and most other spacecraft charging codes is that they use quasi-analytical models for some parts of the calculations, for example for the wake structure, rather than doing a complete particle-in-cell simulation or numerical solution of the Vlasov-Poisson equations for the spacecraft-plasma system. There exist 2D particle-in-cell codes for charging studies [e.g. Usui et al., 1993], and 3D codes are under development, but at present only the semi-phenomenological codes mentioned above are widely available and applicable to practical situations.

POLAR has previously been applied to among others the SPEAR-1 rocket [Katz et al., 1989], the CHARGE-2 rocket payload [Mandell et al., 1989] and to the DMSP satellites [Cooke et al., 1989]. For modelling of Freja charging events, typically at around 1500 km altitude in the auroral zone, POLAR was chosen as the most appropriate tool presently

available, although NASCAP was used as well in some preliminary work [Svensson, 1997]. We have also used the program SUCHGR that is distributed with the POLAR code. SUCHGR is a simplified code modelling the spacecraft as a homogeneous sphere, while POLAR allows detailed modelling of the spacecraft. POLAR and SUCHGR are described in detail in the POLAR User's Manual [Lilley et al., 1989, hereafter referred to as PUM]. In the context of the present study it is necessary to have some knowledge of what POLAR can do and what it cannot, as this clearly is important for understanding the results of the simulations of the Freja charging events. This discussion is given in the following section, where spacecraft charging physics is discussed with particular reference to POLAR.

For the simulations, we have run the POLAR software on Sun workstations (Sparc-5, Sparc-20 and UltraSparc) running Solaris 2.5 and 2.6. For presentation of results, the TRMTLK, SHONTL and PSTPLT packages in POLAR has been used as well as some Matlab routines.

2.2 Current Balance

An object placed in a plasma will always collect some of the plasma particles due to their bulk and thermal motion with respect to the object. A spacecraft in the ionosphere, magnetosphere or solar wind is no exception. In a plasma in thermal equilibrium, the electrons have higher speed than the ions due to their lower mass but equal energy. This causes the flux of electrons to a spacecraft at plasma potential to be greater than the ion flux, causing the spacecraft to charge negatively, unless other effects appear to change this situation. Examples of other effects could be emission of photoelectrons or emission of secondary electrons when the plasma particles hit the spacecraft surface. The presence of non-conductive materials, which may give local charging to parts of the spacecraft, or biased parts like some scientific instruments for particle collection, may also perturb the electrostatic field around the spacecraft in such a way that collection of one particle species is enhanced or decreased. Whatever the situation, at equilibrium the potentials V_k on the surfaces k constituting the spacecraft boundary to space will be such that the total current I to the spacecraft is zero:

$$\sum_{k=1}^{n} I_k(V_1, V_2, \ldots, V_n) = 0 \qquad (1)$$

This may be regarded as the fundamental equation of spacecraft charging. It may be noted that the actual charge distribution, in units of coulombs, on the spacecraft need not be modelled: the surface potentials are completely governed by the current balance equation (1).

One may also note that in general, the current to any surface element will depend on the potentials of all surface elements, as the total set of such potentials determines the potential distribution in space outside the spacecraft, and hence particle trajectories, as well as the flow of currents between surface elements. From now one, we will regard V and I as vectors of n components. The question now is to find the functional form and parameters of the function $I(V)$. From a physics point of view, it is natural to divide the total current $I(V)$ into the contributions from several different processes. For our purposes, it is reasonable to analyse the total current as

$$I = I_i - I_e + I_{ph} + I_{se} + I_{si} + I_c + I_d \qquad (2)$$

where I_i and I_e are the currents due to collection of plasma ions and electrons, respectively, I_{ph} is the current due to photoelectron emission, I_{se} and I_{si} are the currents carried by secondary electrons emitted due to impacts of electrons and ions, respectively, I_c is the current flowing by conduction to adjacent surface elements and to spacecraft bulk, and I_d is the displacement current, which may be important in time-dependent situations. One may also include a term describing the backscatter of impinging particles, but this is almost trivial since it may be described by (energy dependent) coefficients in front of the collected plasma currents. Solving (1) with some appropriate models for (2) may not look like a daunting task, but in fact it is. To find I_i and I_e we need to know the trajectories of particles in the plasma, and thus either calculate the potential field around the spacecraft and track particles through it, or have some other model.

The physics of spacecraft charging will now be discussed by discussing each of these terms in sections 2.3 – 2.6. Particular emphasis will be put on how POLAR treats the problems, as this code has been used for simulation of the Freja charging events. Other terms sometimes included are the ion emission by particle or photon impact, which almost always is negligible, and the backscatter of primary electrons and ions, which always is small compared to the incoming fluxes and also can be modelled by adjusting the incoming fluxes. Artificial beams should need to be included for modelling of Freja charging events where the F6 electron gun [Haerendel et al, 1994] is operational, but no such events has been included in this study.

2.3 Analytical and numerical models

For simple models like a homogeneously conductive spherical spacecraft of uniform surface it may at least sometimes be possible to write down closed-form expressions for *I(V)*, although the presence of shielding and particularly wake effects make even this problem hard to solve [see Al´pert, 1983]. If the plasma is sufficiently tenuous, the electric fields encountered by the particles can be determined from the boundary conditions without reference to other particles in the plasma. In this limit where the Debye length is much larger than the spacecraft size, fields will also decay with distance so slowly that the current is independent of the detailed structure of the field. This is known as the orbital motion limit or OML, for which useful analytical results exist [Mott-Smith and Langmuir, 1926; Medicus, 1962]. Consider a spherical spacecraft (probe) of radius *a* and homogeneous surface properties immersed in an isotropic plasma. We assume the decay of the potential with distance *r* from the centre of the sphere is such that the electrostatic field can be neglected for all *r* outside some value *s*, which we define as the edge of the sheath around the spacecraft. If the plasma is tenuous, *s* may go to infinity. For a particle species with a charge such that the particles are attracted to the spacecraft at potential *V*, the current carried to the spacecraft will be [Mott-Smith and Langmuir, 1926]

$$I = 4\pi q s^2 \int_0^{v_1} v^3 f(v)\, dv + 4\pi q a^2 \int_{v_1}^{\infty} (1 - \frac{2qV}{mv^2}) v^3 f(v)\, dv\,, \qquad qV \le 0 \qquad (3)$$

where

$$v_1^2 = -2\,\frac{a^2}{s^2 - a^2}\,\frac{qV}{m}\,, \qquad (4)$$

q is the particle charge, *m* particle mass, *v* particle speed and *f(v)* the distribution function. We see that if the plasma is tenuous so that *s* is infinite, which is known as the thick sheath orbital motion limit (OML), we get a linear *I-V* relation, whatever the exact form of *f(v)* may be. If *s* is finite, which case is known as the sheath limited case, an extra relation for determining *s* must be supplied, like the Child-Langmuir length law or a numerical solution. For a practical situation in a finite sheath situation, such as a spacecraft charging application, there may appear trapped orbits within the sheath and other complicating factors, and simulation and tracking of particle orbits or numerical solution of the Vlasov-Poisson equations in the sheath is needed.

The code SUCHGR uses the simple model of a spherical spacecraft with no wake effects. For a uniformly conductive spacecraft, results based on such simplifications may often be very good, particularly if the Debye length is large compared to spacecraft dimensions. In other cases, where a spacecraft with many different surfaces and a complicated geometry is to be considered or wake effects are important, more elaborate calculations are needed. Codes like NASCAP and POLAR divide the satellite into a set of *n* surfaces, following the approach of equation (1). To model how the current to any surface depends not only on its own potential but also on the potentials of the adjacent surfaces and the spacecraft bulk, surface resistivities as well as capacitive couplings between surface elements can be modelled.

For modelling a spacecraft-plasma interaction problem with negative charging, POLAR typically starts from user-supplied input on the spacecraft geometry and materials, the plasma parameters and initial potential of the spacecraft. An initial wake structure is determined using geometric shadowing of the spacecraft or a neutral flow approximation. An initial sheath edge is fixed, and using these boundary conditions Poisson's equation for the potential is solved. The motions of test ions are then tracked through the field, and the currents they carry to the spacecraft surfaces are calculated. The currents and densities due to the repelled electrons are calculated using a Boltzmann relation. The response of the spacecraft surfaces to the incoming particle flux is calculated, resulting in a new potential distribution on the spacecraft. This is then used as a new boundary condition for Poisson's equation, which is solved with the ion density found from the tracking process and Boltzmann distributed thermal electrons providing the charge density. Contributions to the charge density from high-energy electrons, secondary electrons, photoelectrons and backscattered particles are not modelled.

Evidently, the space charge limited case is more complicated to handle than OML. However, one may note that outside the sheath edge, OML conditions always apply. If detailed tracking of particle orbits is needed, this has to be done only inside the sheath. This is utilised in POLAR, which switches from OML relations to detailed particle tracking at a presumed well-defined sheath edge, defined by default as $|\Phi| = 0.47\, KT_e / e$. POLAR also has the option of using OML theory only and skip detailed particle tracking. Finally there is a hybrid of the two built into POLAR, where the OML calculation is done for finding the distribution of currents on different parts of the spacecraft, whereafter the total current carried by the attracted species to the spacecraft is normalised to the current through the sheath boundary. This approach promises to significantly reduce the amount of calculations as compared to the detailed

particle tracking in the sheath, but its usage is not well tested or documented [David Cooke, private communication].

In a magnetised plasma, calculating the current-voltage relation for even a simple sphere is very complicated, and few really useful closed-form results exist. POLAR can model the trajectories of the attracted ions taking magnetisation into account. The effects seen when including non-zero magnetic field in the Freja simulations are found to be small, as could be expected as the gyroradii of the attracted ions are greater than the typical spacecraft dimension (about 1 m).

Equation (3) considered the attracted particle species. For a repelling potential, we instead get

$$I = 4\pi q a^2 \int_{\sqrt{2qV/m}}^{\infty} (1 - \frac{2qV}{mv^2}) v^3 f(v)\, dv\,, \qquad qV > 0 \qquad (5)$$

irrespective of sheath thickness. Note that (3) and (5) are continuous at V=0. For the repelled electrons, this analytical result is valid even in a magnetised plasma, and magnetisation can therefore generally be neglected for the repelled species. An exception would be the case where a magnetic field line is cut at two points by spacecraft structures, with plasma open to space in between. However, as discussed below in Section 6, magnetisation may have an impact on the emission of photoelectrons and secondary electrons in conditions of low charging level.

2.4 Photoelectrons

Photoelectron emission from surfaces exposed to sunlight provides an important current in the charging balance for a spacecraft in geostationary orbit or elsewhere in the tenuous magnetospheric plasma. At Freja altitudes, the photocurrent is not as important as in the GEO environment, although it certainly acts to stabilise the spacecraft potential in sunlit conditions. The photocurrent from a surface is fairly simple to model, at least as long as magnetisation effects are neglected. For negative potentials, the photocurrent is essentially independent of the potential: all electrons escape from the surface. This may be changed by the presence of a magnetic field, which may turn some photoelectrons back to the spacecraft even if they are energetically allowed to escape. Laframboise [1988] found that for an infinite planar surface with an angle θ between the surface normal and the magnetic field, the current carried by emitted electrons decreases by a factor $\cos\theta$ if there is no normal electric field at the surface.

If such an electric field is present, the quenching effect becomes less important, and for high voltage charging, here defined as a high value of the ratio of the *E/B* drift speed to the particle speed at emission, the effect is negligible. Also, convex surfaces will be less sensitive than an infinite plane, but locally concave surfaces will on the other hand be more sensitive. The effect may possibly be important for low-level charging events, where the normal electric field is week. POLAR presently does not include this effect, as is further discussed in Section 6.

Another effect suppressing the photocurrent is the formation of electrostatic barriers due to different voltages on different surfaces on the spacecraft, as illustrated in Figure 1. Local potential minima may form in space outside a surface, turning back photoelectrons to the surface. POLAR 1.3.7 includes a simple model of this phenomenon (see Section 6), known to be important in charging in geostationary orbit conditions [Purvis, 1983], where the plasma density is low.

The electrostatic field may also return emitted particles to other points on the spacecraft than they were emitted from. These photoelectrons should be accounted for in the current balance also for the surface where they end up. This phenomenon is incompletely modelled in POLAR 1.3.7 (see section 6).

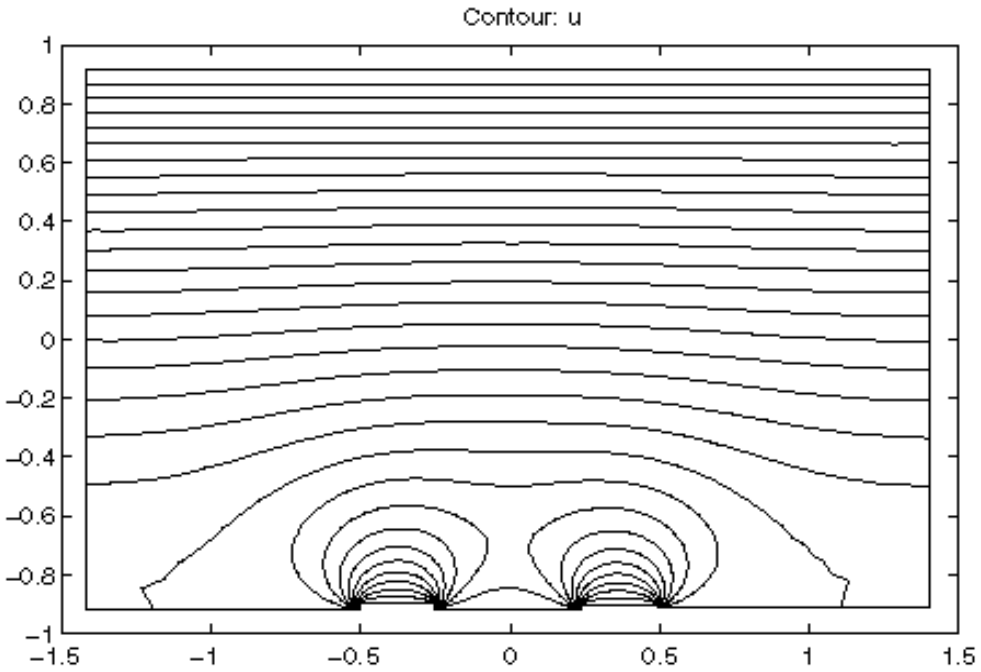

Figure 1. A numerical solution of the two-dimensional Laplace equation above a surface at 20 V with two small segments at 30 V. Equipotential lines with 2 V separation are shown. The potential is put to zero at the upper boundary, and the horizontal electric field is zero on the right and left boundaries. The formation of a local potential maximum of a few volts in space between and above the two small plates at 30 V is evident. Such a potential can form a barrier for particles expelled from the surface between the two small plates with energy below the magnitude of the potential barrier.

2.5 Secondary electron emission

When an electron or ion hits a surface, one or several other electrons may be emitted from the material, usually at fairly low energy (a few eV). The number of electrons emitted for each incoming particle is known as the yield Y. For incoming electrons, Y strongly depends on their energy E. The yield curve $Y(E)$ is obviously zero for zero energy and also zero for infinite energy (as very high energies give very limited possibility of interaction), so there must be at least one maximum in between. Experimentally, most materials are found to have one maximum in the yield curve, at a few hundred eV (compare Figure 7). The maximum value of Y may well exceed one: for aluminium, the peak yield is 0.97, while it is around 3 for Teflon. Thus secondary electron emission may be very important to the current balance for a spacecraft. A corollary is that simulations and calculations of spacecraft potential will be sensitive to errors in the model used for describing the secondary emission [Katz et al., 1986].

The fact that the secondary yield curve is peaked opens up for the possibility of bifurcated equilibria in spacecraft charging physics. Consider the simple case of a conductive spacecraft in a plasma only consisting of monoenergetic isotropic electrons at some energy E. In the case of orbit limited current collection, the current of electrons hitting the spacecraft will be a linear function of the spacecraft potential V [Medicus, 1961], like the solid line in Figure 2. In this simplified case, the hot electron current must be balanced by the secondary current, which depends on $E + eV$, which is the energy of the electrons when hitting the spacecraft. The secondary current thus is a peaked function of V, like the dashed line in Figure 2. The simple sketch in Figure 2 shows the possibility of two points where the currents balance each other, and thus of two equilibrium potentials in this case. In addition, any potential below $-E/e$ is an equilibrium in this oversimplified case: in a more realistic situation [e.g. Lai, 1991], this continuum of roots would collapse to a single root. In such a case, which equilibrium actually is attained will depend on the history of the spacecraft-plasma interaction and not only on the instantaneous and local parameters.

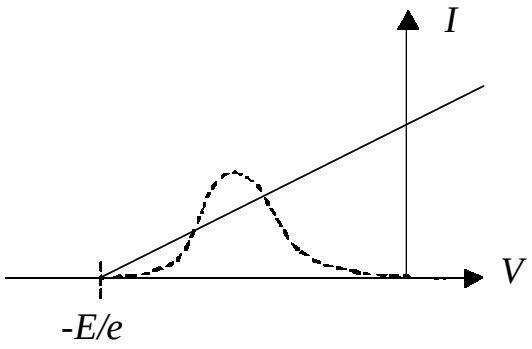

Figure 2. Schematic of a situation with only hot monoenergetic electrons at energy E (solid) and secondary emission (dashed). There are three possible equilibria: at any potential $V < -E/e$ and at the two intersection points.

POLAR includes the NASCAP algorithms for calculation of secondary currents. The inputs needed are properties of surface materials and spectra of incoming primary particles. All materials known to NASCAP are included in POLAR, and for this study a number of other material specifications provided by ESTEC have also been used. As is the case with photoelectrons, POLAR looks at the secondary electrons only as a term in the current balance: they are not tracked out in space and do not contribute to the calculated charge density in the plasma. The treatment of current suppression due to potential barriers is similar that applied to photoelectrons (Section 2.4).

2.6 Charging dynamics

Dynamic effects may enter the spacecraft-plasma interaction on two levels. The first and simplest level is when the boundary conditions in the plasma or for the spacecraft change so slowly that the sheath appears constant to the particle on a time scale it traverses the sheath. Dynamic effects on this time scale can be treated by introducing a displacement current in equation (2), thus requiring knowledge of the relevant capacitances. This can be a complicated task, as unless all parts on the spacecraft are conductors in contact with each other, there will be internal capacitances within the spacecraft. The spacecraft-plasma interaction may in this situation be modelled as a sequence of quasi-steady states, which is the approach taken by NASCAP and POLAR. The user must explicitly provide the internal capacitances between various parts of the spacecraft, while external capacitances to the plasma are modelled by the code.

The second and more advanced level for treating dynamical situations would be to consider not only quasi-steady states but also the real dynamics of the plasma itself, down to Debye length and plasma oscillation scales in space and time. This would allow the modelling of wave generation and other time-dependent plasma phenomena, but would require a full plasma simulation of the interaction, which would be very costly in terms of computer power.

Correct treatment of charging dynamics including internal capacitances may be very important when studying the formation of differential charging on a spacecraft, which eventually may lead to an arcing discharge. Our chief interest is the final equilibrium state of the overall satellite potential configuration, and we therefore do not attempt to model the charging dynamics. In particular, no estimate of internal capacitances is included in the calculations. For numerical reasons, a short timestep has to be used in the simulations, but we do not attempt to interpret the timescale we use as necessarily corresponding to the real charging timescale. One may note, however, that the charging timescale for Freja is observed to be short (on the order of a few milliseconds; c.f. WP110).

3. THE FREJA SPACECRAFT

This section covers the aspects of Freja relevant for this spacecraft charging simulation study, and presents a modelling of Freja for POLAR. For a more detailed description of Freja and the instruments carried on it we refer to André [1993] and Lundin and Haerendel [1994]. We first review the general design in Section 3.1. The materials used on Freja are then listed in Section 3.2. The Freja models for use with POLAR are described in Section 3.3.

3.1 General Freja design

Freja (Figures 3 – 6) is a sun-pointing spacecraft with solar panels placed on a flat circular surface. The overall diameter is 2.2 m. The solar panel platform constitutes the "upper" deck or platform. The "lower" deck is connected to the upper via a central aluminium tube. Radially from this tube four support webs are mounted between the decks. The lower deck is 1.2 m in diameter. The distance between the two decks is 0.44 m.

In the central tube two solid powered motors are mounted, one facing "upwards", one facing "downwards", which were used to lift the spacecraft into its final orbit. Each motor has a nozzle made of composite material. The conductive properties of these nozzles, which are dielectrics on ground, are not well known, but a carbonization effect during their use is assumed to make at least their inner surface conductive. We have in this study represented them by the conductive material CFRP (see then next section) and a variation of this material with very low conductivity. The space between the decks is partitioned by the support webs into four distinct compartments known as instrument bays, where the different booms, scientific instruments and other system units are mounted.

An important design goal was to have as much as possible of the outer surface electrically conductive in order to cancel electrical charges induced by the plasma environment and prohibit differential charging. It is not possible to achieve a 100% coverage of the surface with conductive material, as insulating material must be used for certain purposes, such as insulating an electrostatic probe from the satellite. The total area of exposed insulators on Freja is about 0.38 m^2 (including engine nozzles) which may be compared to the thermal blanket exposed area of about 5.5 m^2.

The basic structure of the spacecraft is made of honeycomb aluminium. Structure elements

extending outside blankets are painted with white paint of type PCB-Z, assumed to be conductive in space.

The eight identical solar panels are each covered by solar cells of 0.19 m^2 area, giving a total solar cell area of 1.52 m^2. A transparent conductive coating of indium tin oxide (ITO) is applied to the solar panels in order to ensure conductivity.

To keep the temperature within desirable limits, and to provide a conductive outer coating, a large part of the spacecraft including most of the instrument bays are covered by Sheldahl thermal blankets of aluminised Kapton with ITO coating.

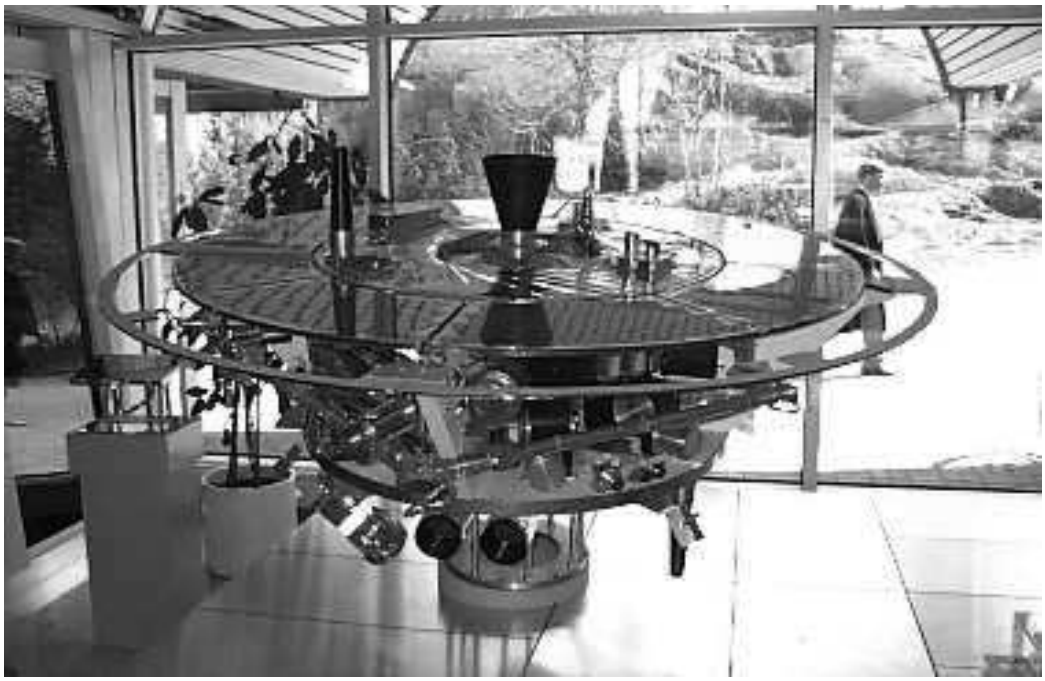

Figure 3. The Freja mockup at the entrance hall of the Swedish Space Corporation in Solna, showing the essential features of Freja. In flight configuration, thermal blankets covered the instrument bays.

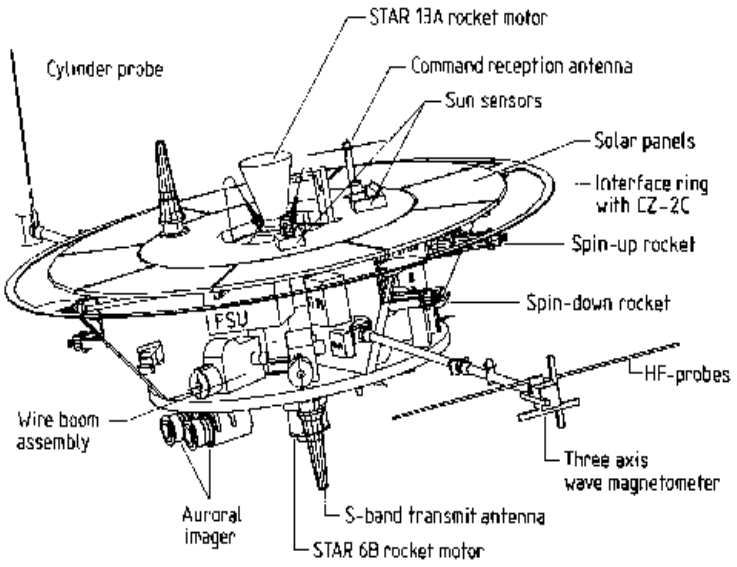

Figure 4. Some instruments and equipment on Freja. From André et al [1993].

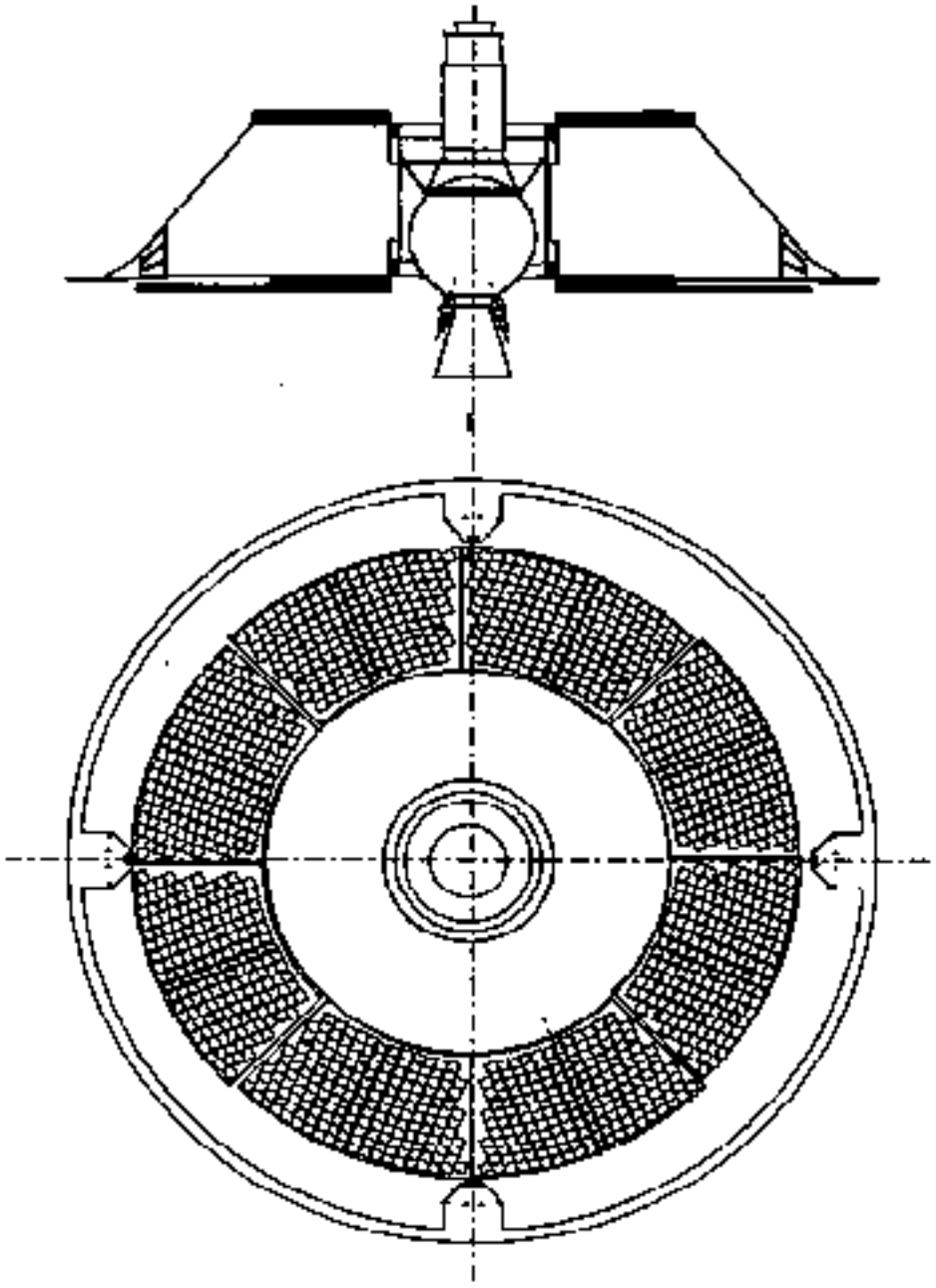

Figure 5. Freja structural concept. From André et al [1993].

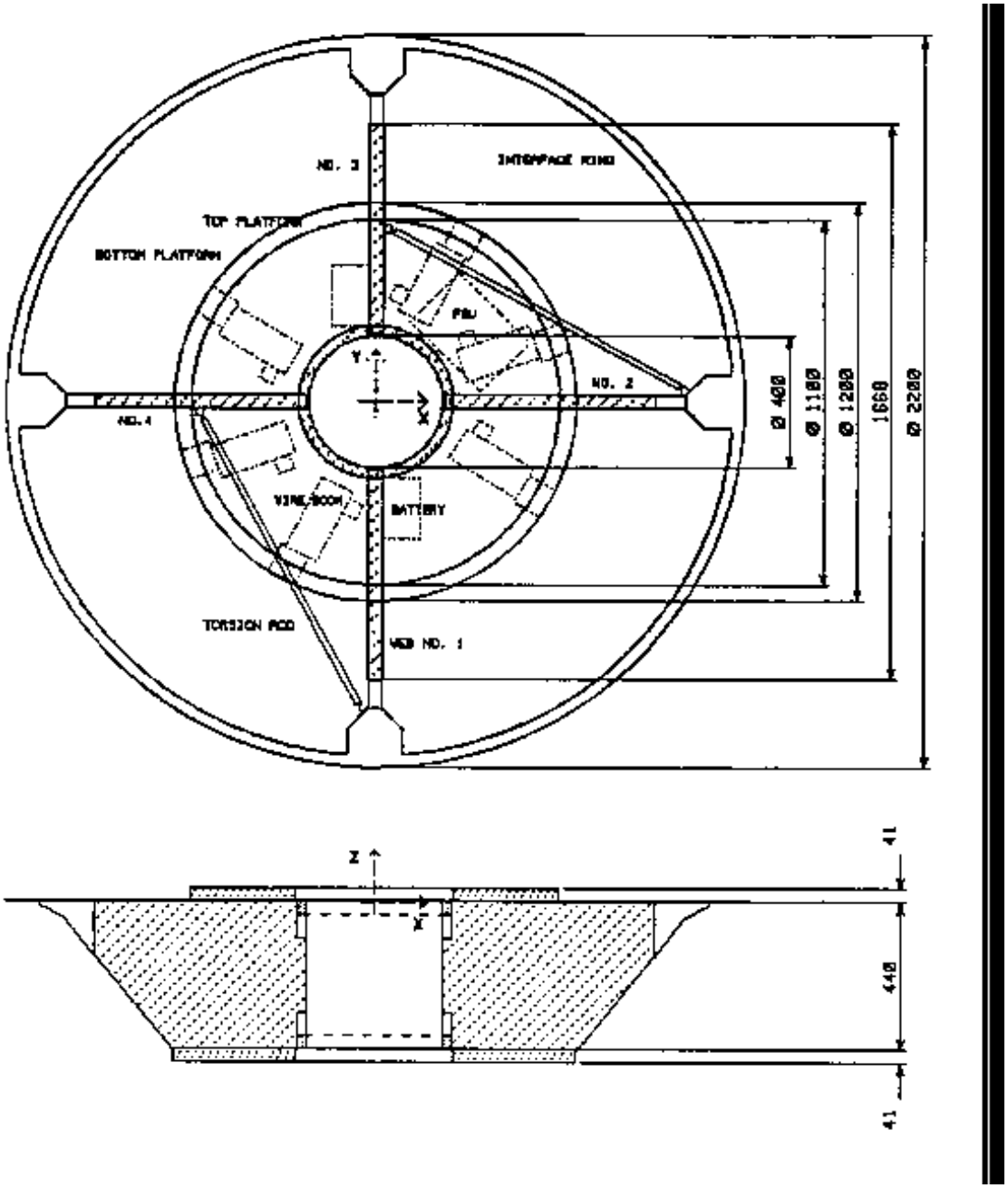

Figure 6. Primary structure and spacecraft coordinate system (not identical to model coordinate system in the simulations). Dimensions are in mm. From André et al [1993].

3.2. Freja surface materials

In order to accurately model the spacecraft, we must know the properties of its exposed surfaces. A detailed investigation of the Freja satellite has been performed, and a materials list (Appendix A) has been compiled. A summary of the major surface materials is found in Table 1. Names of model materials for the POLAR simulations are also given in the table. These model materials are further discussed below. For purposes of spacecraft charging, the exposed insulators are of particular interest. These are listed in Table 2.

Part	**Material**	**Model material**	**Area [m^2]**	**Comment**
Instrument bays	Thermal blanket	BLAN	2.8	Thermal blankets covering scientific instrument electronic units and system units. Some exposed detectors.
Top and bottom platforms	Thermal blanket	BLAN	2.7	
Solar panels	ITO coating	ITOC	1.65	
Central tube inner mantle	Thermal blanket	BLAN	1.1	
Support webs (four)	Painted aluminium	PCBZ	4 x 0.7	Only exposed outer parts are painted and included in the area estimate.
Interface ring	Al	ALUM	0.5	Approximated as 2D ring, r = 1100 mm, dr = 37 mm
Main engine STAR 13A body	Titanium	ALUM	0.4	Considered as mantle of cylinder r = 154 mm, h = 396 mm.
Solar cell support	Painted aluminium	PCBZ	< 1.65	Some area covered by support webs and bay blankets.
Sun sensors	ITO coating	ITOC	2 x 0.05	One on top, one on bottom platform. Approximate dimensions 0.1 x 0.1 x 0.1 m.
TM antennas	Carbon fibre	CARB	2 x 0.05	One each on top and on bottom platform. Considered as cylinder r = 50 mm, h = 340 mm. Assumed insulator in this study.
Main engine nozzle	Carbon fibre	CARB	0.3	Considered as cylinder of radius 150 mm, h = 240 mm. Assumed insulator in this study.
Bottom engine STAR 6B	Aluminium	ALUM	0.02	

Table 1. Materials of major exposed surfaces on Freja. The "model material" refers to the baseline input for POLAR simulations (models Ar and Cr below); variations have also been used.

Item	**Surface area** [m^2]
External parts of equipment bay:	
LSL Coax	0.0001
Separation switch harness	0.0300
Coax switches	0.0036
Power splitter	0.0009
Coaxes	0.0144
TICS cable	0.0020
Arming plugs	0.0020
DC-magnetometer boom:	
DC probe harness	0.0023
Cable loops	0.0075
CYLP pyro	0.0018
Search Coil Magnetometer boom:	
HF pyro	0.0018
Bottom platform:	
Lower TM antenna cover	0.05
S-band antenna coax	0.0050
Kevlar retention string	0.0004
TESP cradle rubber	0.0006
TESP rubber support	0.0010
TESP cables	0.0050
TESP backshell	0.0020
TESP pyro	0.0015
TESP kevlar string	0.0004
LSL antenna base	0.0015
MATE cable	0.0045
MATE cradle support	0.0004
STAR 6B nozzle	0.0100
Top platform:	
Upper TM antenna cover	0.05
S-band antenna coax	0.0050
Kevlar retention string	0.0004
STAR 13A nozzle	0.1200
STAR 13A harness	0.0150
Solar panels:	
Brackets	0.0058
Rear side cabling	0.0110
Top side TCC	0.0180
Edge TCC	0.0285
Total area including nozzles:	**0.38**
Total area excluding nozzles:	**0.24**

Table 2. List of exposed insulators on Freja. The list also includes the engine nozzles, as the impact of a possible non-conducting surface on these is assessed in the study.

Number	Symbol	Description	Unit
1	ε	Relative dielectric constant	1
2	c	Thickness of dielectric material	m
3	s	Bulk conductivity (-1 for metallic conductor)	S/m
4	Z	Atomic number	1
5		Maximum secondary electron yield for electron impact	1
6		Primary electron energy that produces maximum secondary yield	keV
7	P_7	Penetration depth parameters: $R=P_7 E^{P8}+P_9 E^{P10}$	Å
8	P_8	[PUM page 4.5-6]	1
9	P_9		Å
10	P_{10}		1
11		Secondary electron yield due to impact of 1 keV protons	1
12		Incident proton energy that produces maximum secondary electron yield	keV
13	j_{ph0}	Photoelectron yield for normally incident sunlight	A/m^2
14	S	Surface resistivity (-1 for perfect insulator)	W/square
15		Maximum potential attainable before a discharge must occur	V
16		Maximum potential difference between surface and underlying conductor before a discharge must occur	V

Table 3: List of material properties to specify for POLAR simulations. See PUM page 6.1-41. Actually used values of these parameters are listed in Appendix B.

For correctly calculating the charging and discharging of dielectrics and the photocurrents and secondary currents, POLAR needs a specification of the material of each surface in the spacecraft model it uses. The principal properties we need to know for each material are specified in Table 3, listed in the order they appear in the material specifications for NASCAP and POLAR [PUM p. 6.1-42]. Laboratory values of these parameters for some materials are available directly in the NASCAP and POLAR codes. Other material parameters have been supplied by ESTEC based on measurements at DERTS.

For the POLAR simulations of Freja charging events, the following materials have been used to model the satellite:

ITOC Indium tin oxide (ITO) coating. The secondary electron yield for materials with this coating has in laboratory tests been found to be rather independent of the underlying bulk material. In our case, the ITOC is applied on the solar panels.
Source: ESTEC

BLAN Thermal blankets of Sheldahl fabrication. Aluminised Kapton with ITO coating.
Source: ESTEC

ALUM Aluminium for some spacecraft structure parts, particularly interface ring. The values we use are for pure aluminium surfaces. In reality, oxidisation will increase the secondary electron yield.
Source: NASCAP.

PCBZ White paint assumed conductive in space, applied to most aluminium areas which otherwise would have been directly exposed.
Source: ESTEC

CPAI NASCAP conductive paint specification. Used as replacement for PCBZ in some simulations in order to see effects of material parameter variation.

CFRP Conductive carbon fibre material, used to model the engine nozzles and some details.
Source: ESTEC

CARB This material has been constructed for simulating the behaviour of non-conductive carbon fibre. We use the parameters for CFRP above, with bulk conductivity and surface resistivity replaced by CONT values.

CONT A generic for dielectric materials having been exposed to the space environment. In laboratory tests, the secondary yield properties were found to be rather independent of which dielectric it was, so we use this for modelling of all dielectrics except carbon fibre parts.
Source: ESTEC

Complete listings of the material parameters of these model materials are given in Appendix B. The most important feature of the materials for this study is their secondary electron emission. Plots of the secondary yields are shown in Figure 7, which also shows the yield curves for Teflon (source: ESTEC).

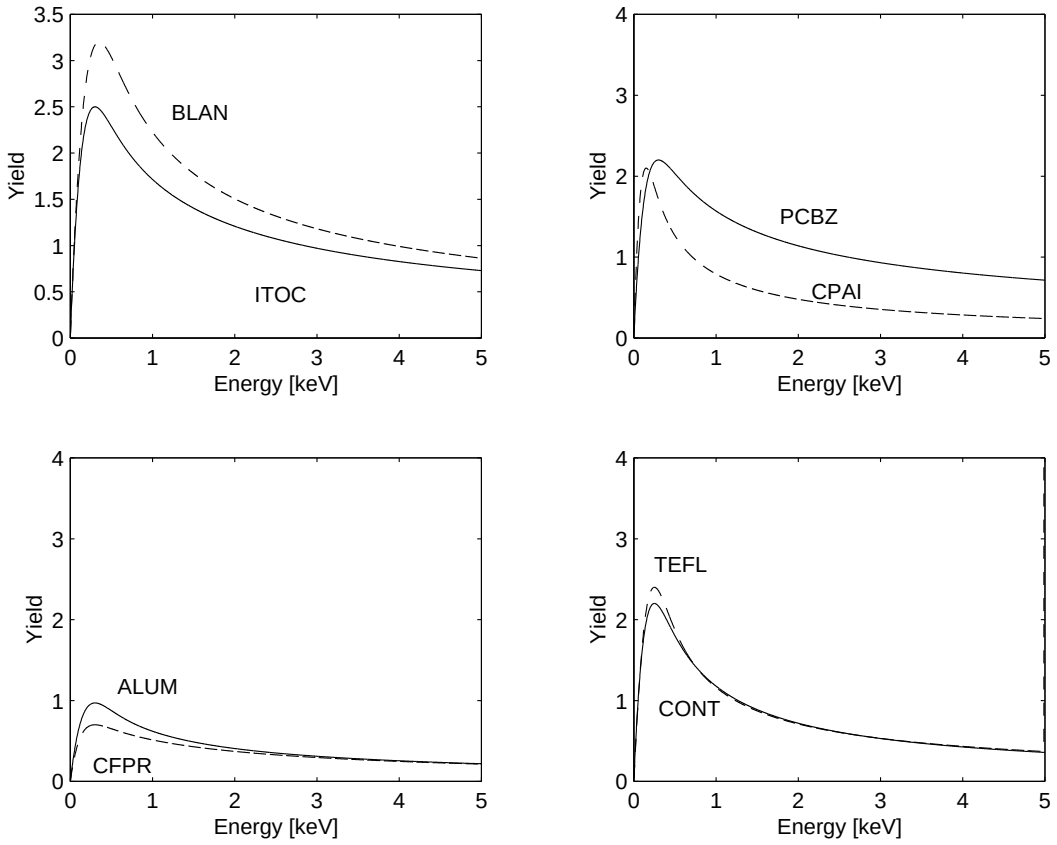

Figure 7**.** Secondary yield curves for materials used in the Freja model.

3.3 Freja models for POLAR simulations

In POLAR, a spacecraft is modelled in a fixed grid of cubical elements. Except for the additional ability of NASCAP to model one-dimensional structures (i.e., booms) as well as the two-dimensional (rectangular plates and slanted triangular surfaces) and three-dimensional (cuboids, octagons, wedges etc) objects possible to model in POLAR, the two programs are similar in terms of spacecraft definition. For a detailed description of how to model a spacecraft in POLAR, see PUM sections 6.10–6.14.

In order to test the effects of geometric details in the simulation software, spacecraft models on three levels of sophistication have been used. The basic versions of these three geometric models, known as A, B and C in order of increasing geometric complexity, are outlined below. In the actual simulation runs, the models have been varied in terms of material definitions and slight geometrical changes in order to estimate the effects of such changes. The geometries of the models are seen in Figures 8 – 11, which are made by the POLAR spacecraft definition module, VEHICL. The input files (called fort.20 in the POLAR file structure, see PUM Section 5.30) defining the models are reproduced in Appendices C, D and E. These files also includes extensive comments providing additional information on the definition of the Freja models for this study.

For each of the geometrical models, we may vary the choice of material and material properties for the surfaces of the satellite in order to check the influence of surface material parameters. This leads to several sub-models, called Am, Cn, Cp etc. The relation between these models is explained in Table 4. The baseline models are Ar and Cr, which incorporates the best knowledge of the spacecraft we have. Model Am is a simple effort to model a worst-case situation of magnetic field inhibition of secondary electrons, by simply reducing the secondary and photoelectron yield for all materials to 2/3 of their nominal values. Models Aq and Cn replace PCBZ by CPAI. As can be seen in Figure 7, this significantly decreases the secondary yield, and should thus make the spacecraft more prone to charging. There is no deep thought behind this model, just a check of the impact of changing material parameters. Model Cp is similar, except that there are no non-conducting areas on nozzles.

Ar, Cr	Baseline material choice. Uses CARB to models non-conductive parts of nozzles, and CONT to model other insulators. Conductive paint is PCBZ.
Am	All secondary yield values reduced to 2/3 of table values to model worst-case effect of magnetic suppression of secondaries. No insulators included.
Aq, Cn	PCBZ replaced by CPAI to study effects of variations of material parameters.
Cp	As Cn but nozzles conductive.

Table 4. Differences between different Freja models.

Model A is a simple definition of the spacecraft as a rectangular object of 2x1x2 grid units (Figure 8). This very simple model is used (a) for testing the plasma environment models on a simple object requiring comparatively little computational effort, and (b) for comparison to the results from Model C in order to test the effects of geometrical details, simulation grid size and small surfaces of non-conducting materials.

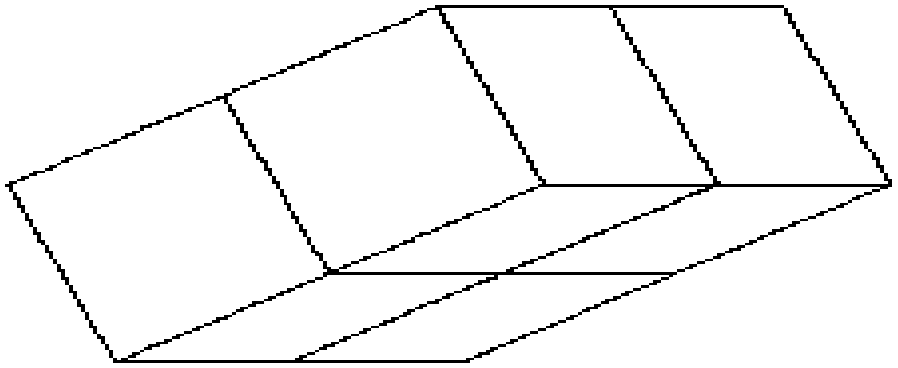

Figure 8**.** Geometry of Freja model A.

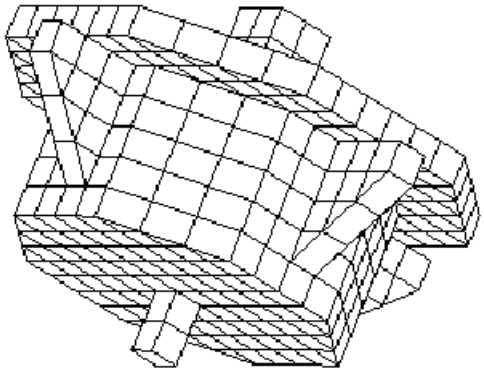

Figure 9. Geometry of Freja model B.

Model B uses a spacecraft definition grid size of 17 x 17 x 33 cells, which was the limitation of previous versions of POLAR. This leads to a grid unit length of approximately 16 cm for Freja. A version of this model was first used in preliminary runs in May 1997 [Svensson, 1997], and later for comparisons to Models A and C for some events. The model incorporates the main features of Freja (Figure 9) with possibility to model some details. It is listed in Appendix D and was constructed from the following geometrical elements:

1. Solar panels: Modelled as an octagon of height 1, width 14 and side 6 in grid units, axis along y axis from y=0 to y=1.

2. Top platform and central tube: Octagon of height 5, width 10 and sides 4, with axis along y axis from y=0 to y=5. This overlaps with the solar panels, thereby defining the top platform. This makes it possible to have different materials for solar panels and top platform.

3. Support webs: Each modelled as a rectangle plus a wedge. Total height 4 units, extension in x or z directions 3 units, thickness in the remaining direction 1 unit.

4. Bottom platform: Octagon with axis along y axis from y=5 to y=6, width and sides as for top platform.

5. Top nozzle: Rectangular, of size 2 in the x and z directions and 3 in the direction, on top of the top platform (-3<y<0).

6. Bottom nozzle: Rectangular, of size 1 in the x and z directions and 2 in the direction, under the bottom platform (6<y<8).

Model C is the most detailed, with a grid size of 10 cm, allowing additional detail (Figures 10 and 11). The difference to model B (15.7 cm grid spacing) may seem small, but is sufficient to allow modelling of gaps in the satellite geometry, e.g. the space between the rocket engine and the central tube and the space between the solar panels and the interface ring. One should also note that the improvement of linear geometric resolution by a factor of 15.7/10 = 1.57 from model B to model C implies an area resolution improvement of 1.572 = 2.5, offering extended possibilities for the study of effects small patches of insulating material.

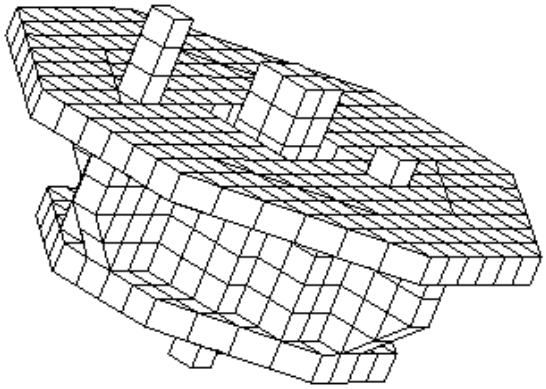

Figure 10. Geometry of Freja model C (top view).

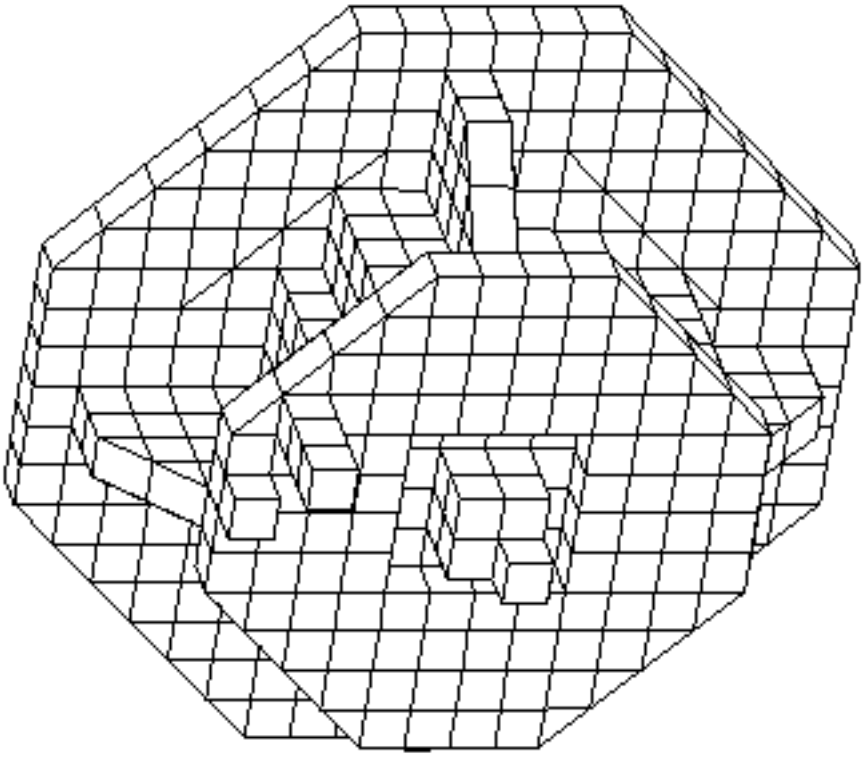

Figure 11. Geometry of Freja model C (bottom view).

POLAR 1.3.7 allows a grid size of up to 50 x 50 x 100 points for the definition of the spacecraft. However, a maximum number of 1250 simple surfaces can be handled, which means that for any reasonably spherical or disc-like spacecraft, the full number of grid points can never be used. For Freja, with a diameter of 2.2 meter, geometrical restrictions alone would allow a resolution of less than 5 cm in grid size, but due to the need to keep the number of surface elements low, the grid resolution of 10 cm used in Model C is the smallest that can be used in practice.

Model C is constructed from the geometrical elements described in the list below. The complete model definition is found in the object definition file frejaC.obj for POLAR (Appendix E).

1. Central tube. This is described as a rectangular funnel structure extending over $-4<y<0$, with outer dimensions 6x6 grid units in the *x* and *z* directions and of thickness 1. Smoothing wedges are applied in the inner corners.

2. Lower platform. An octagonal platform in the *xz* plane, $-5<y<-4$, with a square hole for the central tube.

3. Upper platform. Similar to the lower platform.

4. Support webs: Each modelled as a rectangle plus a wedge. Total height 4 units, extension in *x* or *z* directions 5 units, thickness in the remaining direction 1 unit.

5. Solar panels. Defined by two concentric octagons, the inner one being the upper platform and the outer lying 3 grid units further out, in the same plane as the upper platform.

6. Engines. These are modelled by a rectangular structure of width 2x2 in the *xz* plane, extending for $-7<y<3$. Lowest part is 1x1 wide to simulate lower engine small nozzle.

7. Thermal blankets in instrument bays. Blankets cover most of the payload and spacecraft system located between the platforms. These are modelled as one 2x2 and one 3x1 unit cuboid in each quadrant, extending all the way between the platforms $-4<y<0$.

8. Spacecraft system units: TX antennas and sun sensors added to top and bottom platforms. Modelled as 1x3x1 and 1x1x1 cuboids, respectively.

Onto this basic spacecraft system, one can add cuboids representing other details in the payload or satellite system units. It is particularly interesting to consider the effect of insulting materials, which may be modelled as follows (compare Table 2):

9. Upper platform insulators. These add up to some 8 dm^2 in total area, not counting the rocket nozzle.

10. Bottom platform insulators. Add up to about 2 dm^2.

11. Other insulating material (mainly due to harness) adds up to about 7 dm^2, which may be modelled by distributing 2 dm^2 of CONT on each of the thermal blankets between decks.

Figures 12 – 19 show how the materials described in Section 3.2 have been distributed on spacecraft models A and C. For model C, care has been taken to get the total area of the insulators closely approximating the values in Tables 1 and 2. For the crude model A, the dielectric surfaces are exaggerated in size. The complete definition of the models, including additional comments on how the materials have been distributed, are contained in Appendices C, D and E.

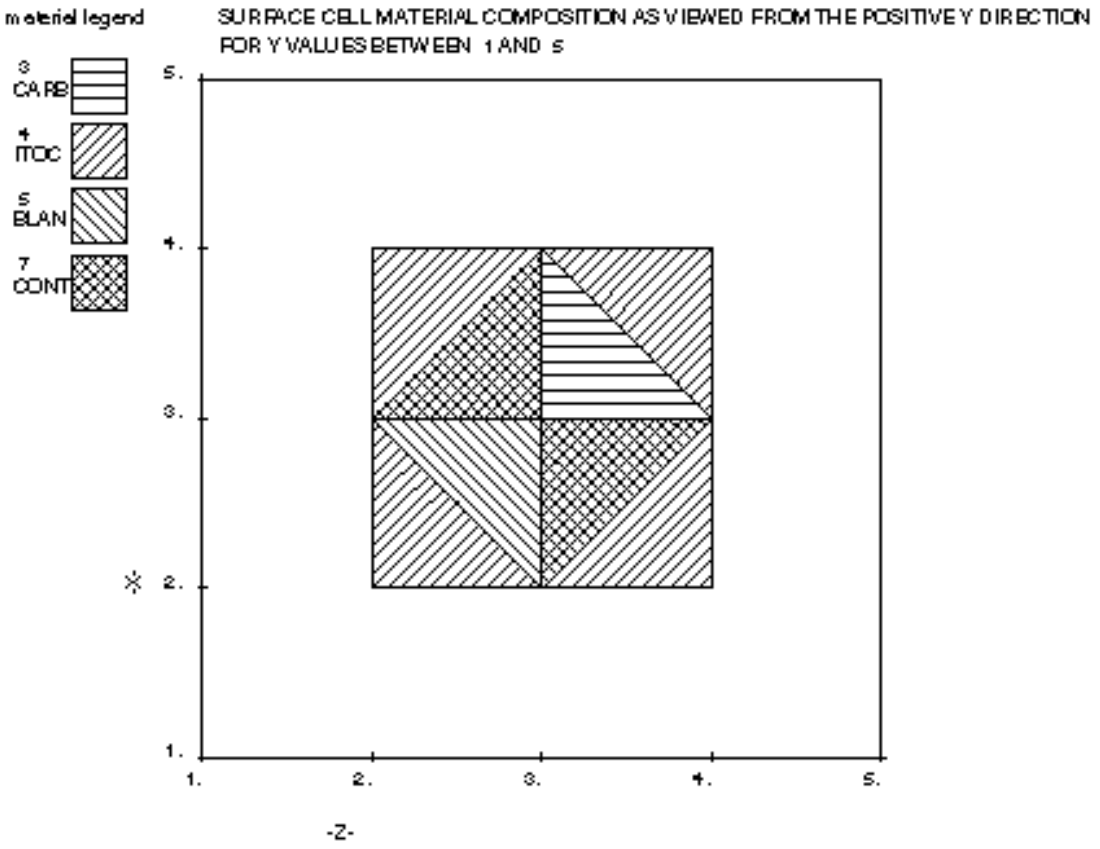

Figure 12. Distribution of materials on model Ar as viewed from the positive y direction (upper platform and solar panels).

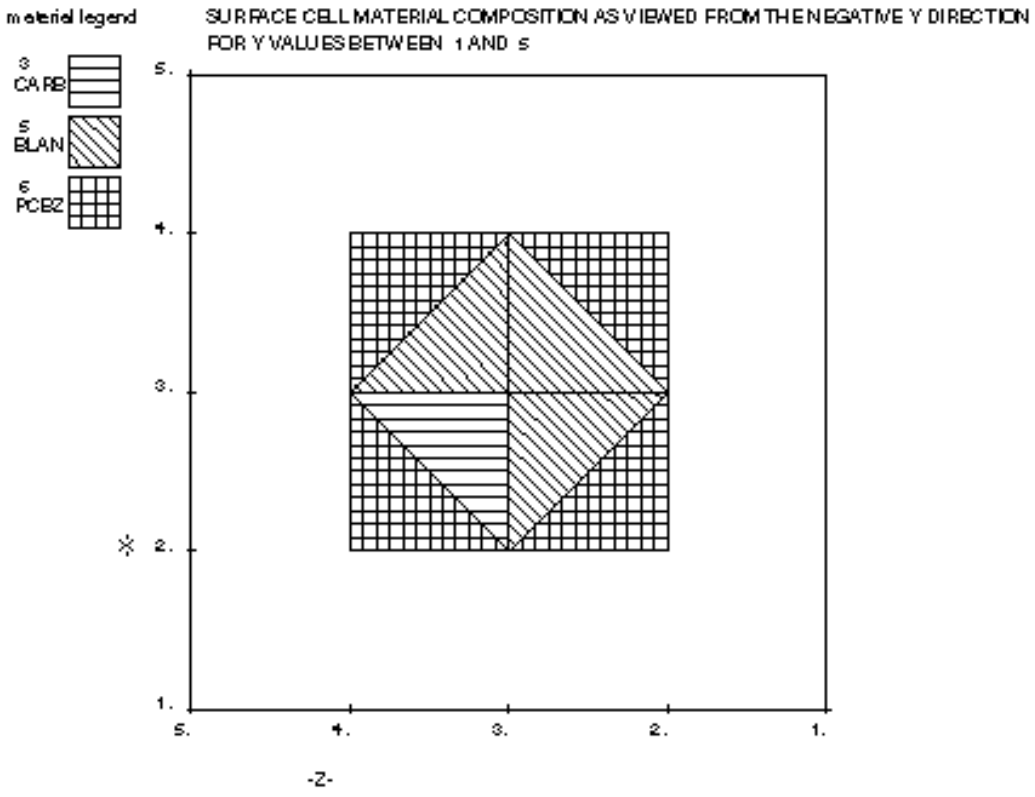

Figure 13. Distribution of materials on model Ar as viewed from the negative y direction (lower platform).

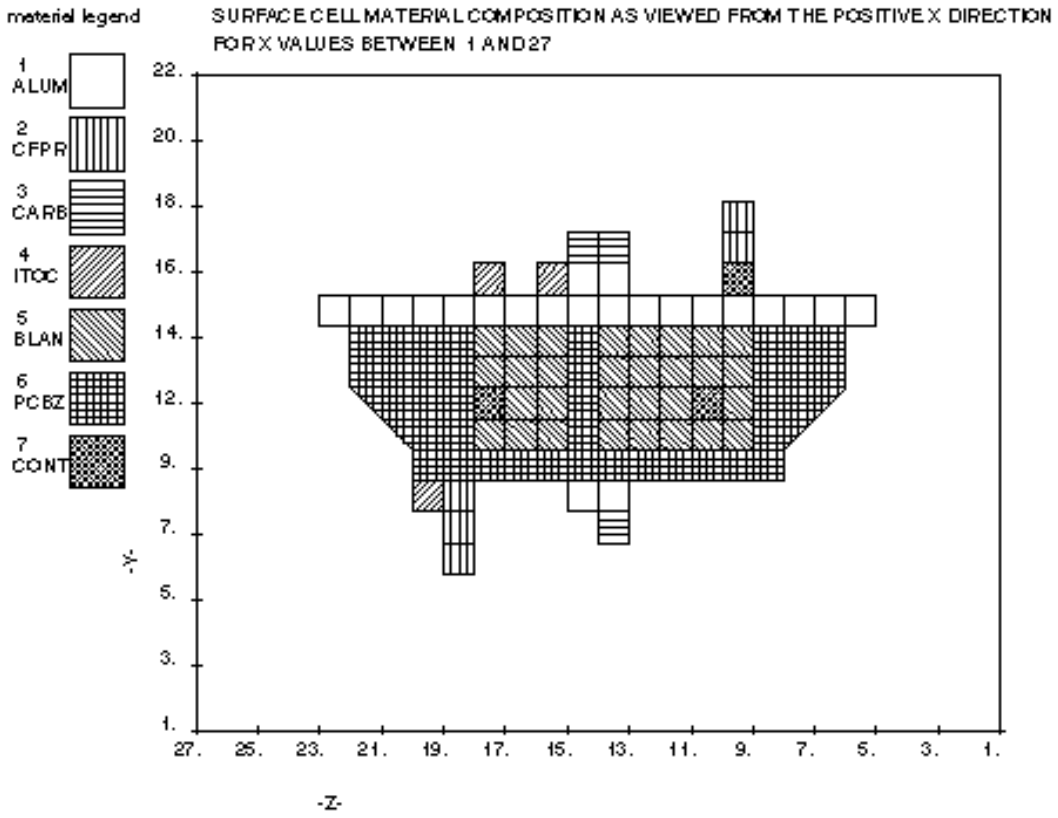

Figure 14. Distribution of materials on the +*x* side of model Cr.

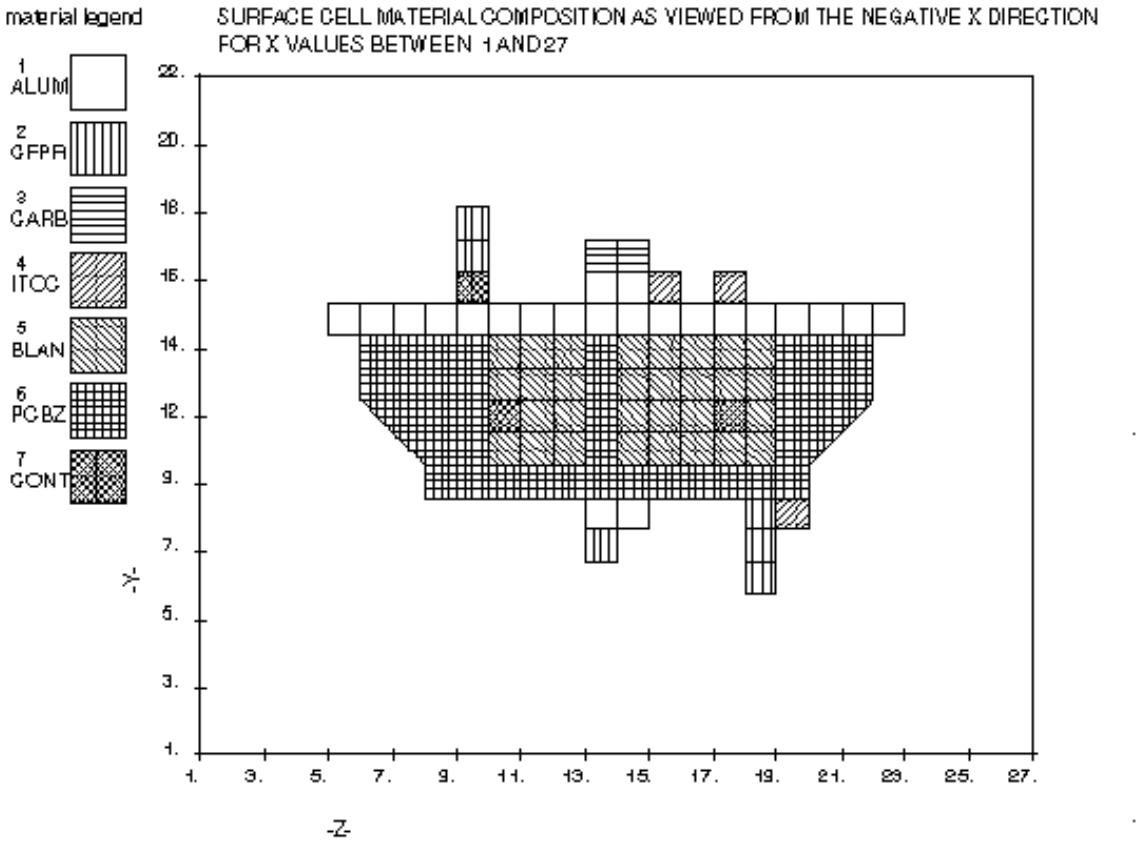

Figure 15. Distribution of materials on the -x side in model Cr.

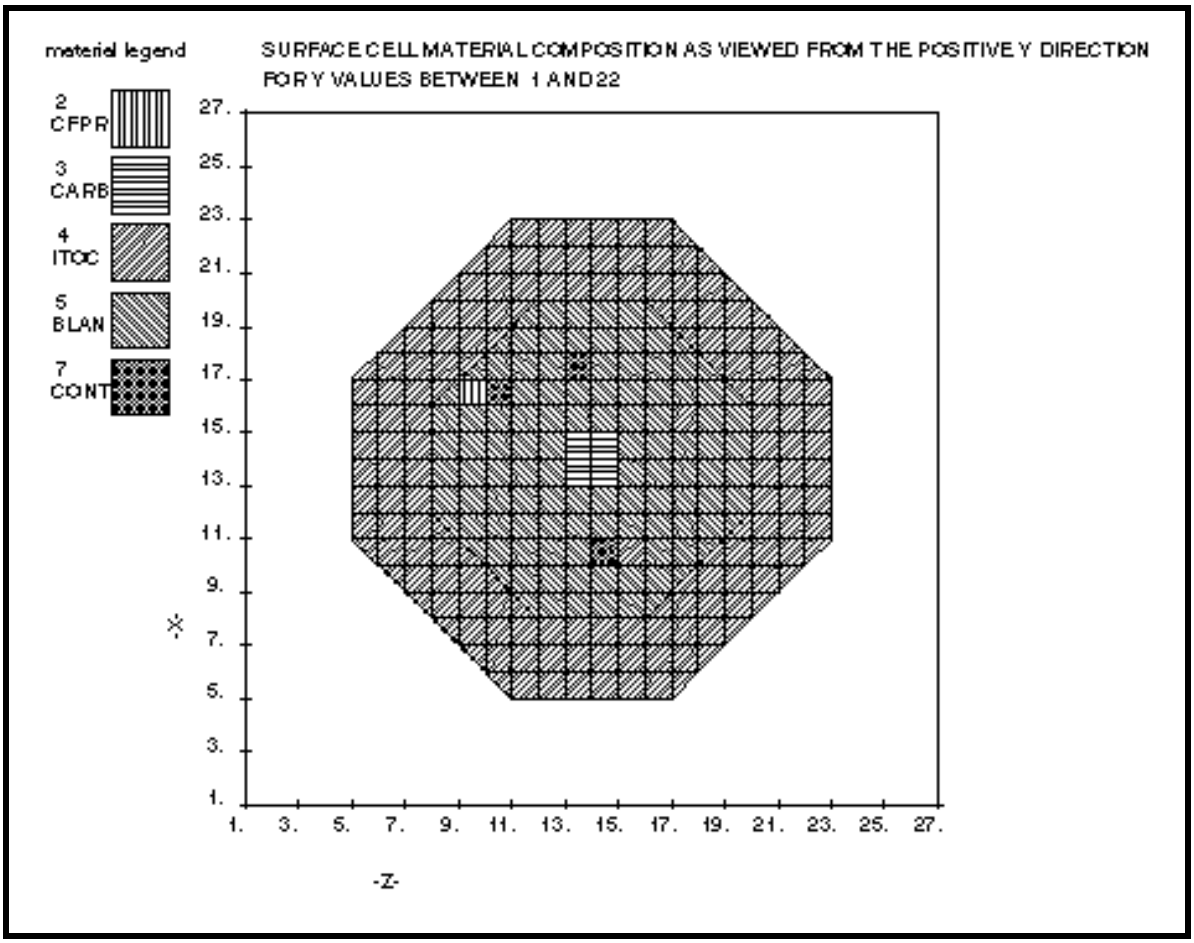

Figure 16. Distribution of materials on the +y side in model Cr.

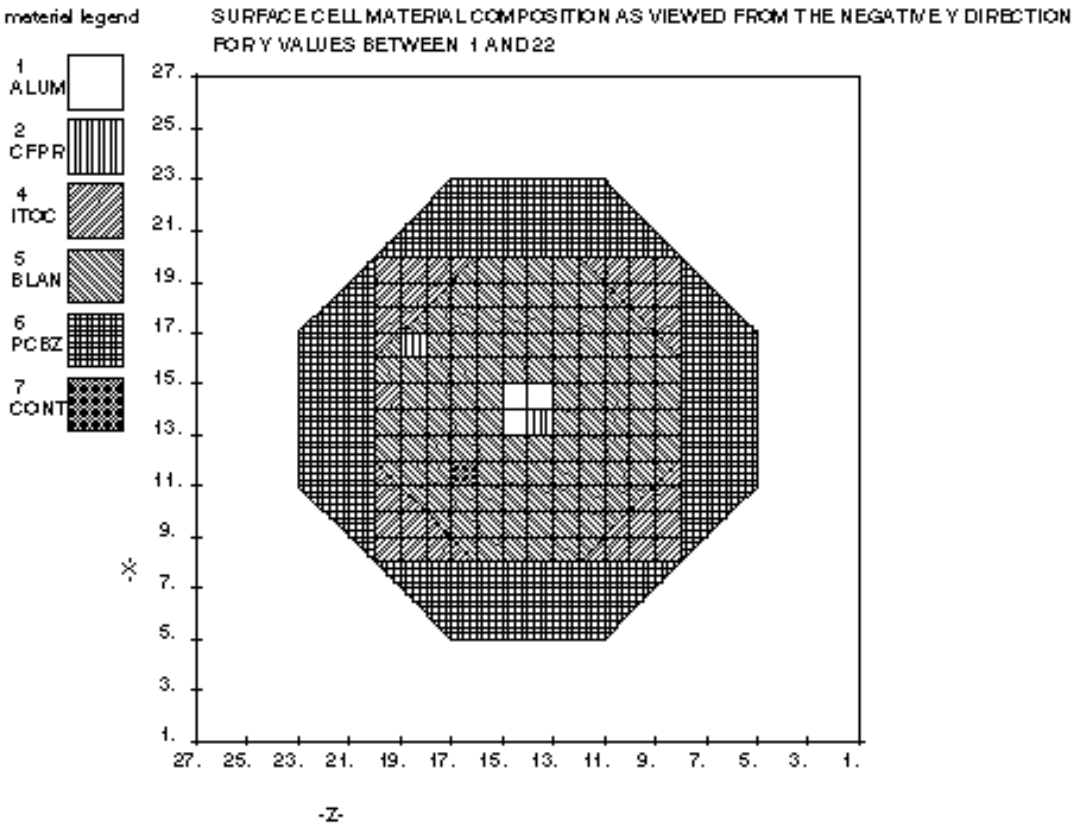

Figure 17. Distribution of materials on the -y side in model Cr.

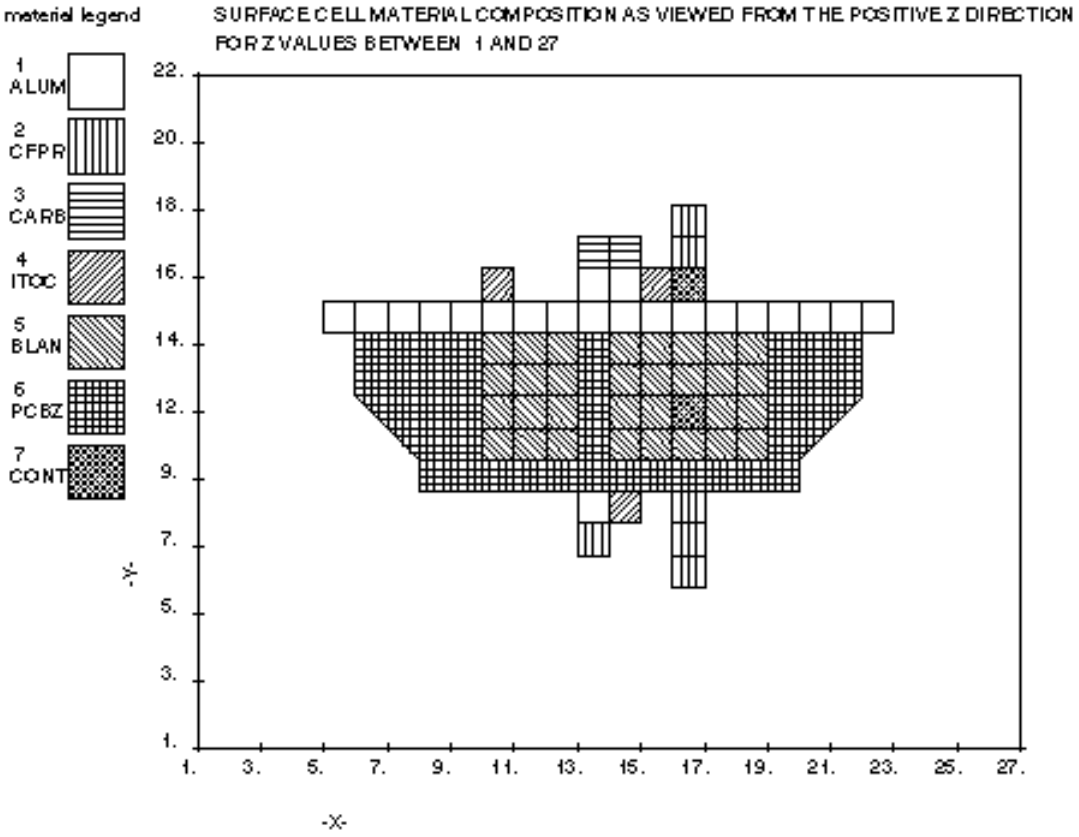

Figure 18. Distribution of materials on the +z side in model Cr.

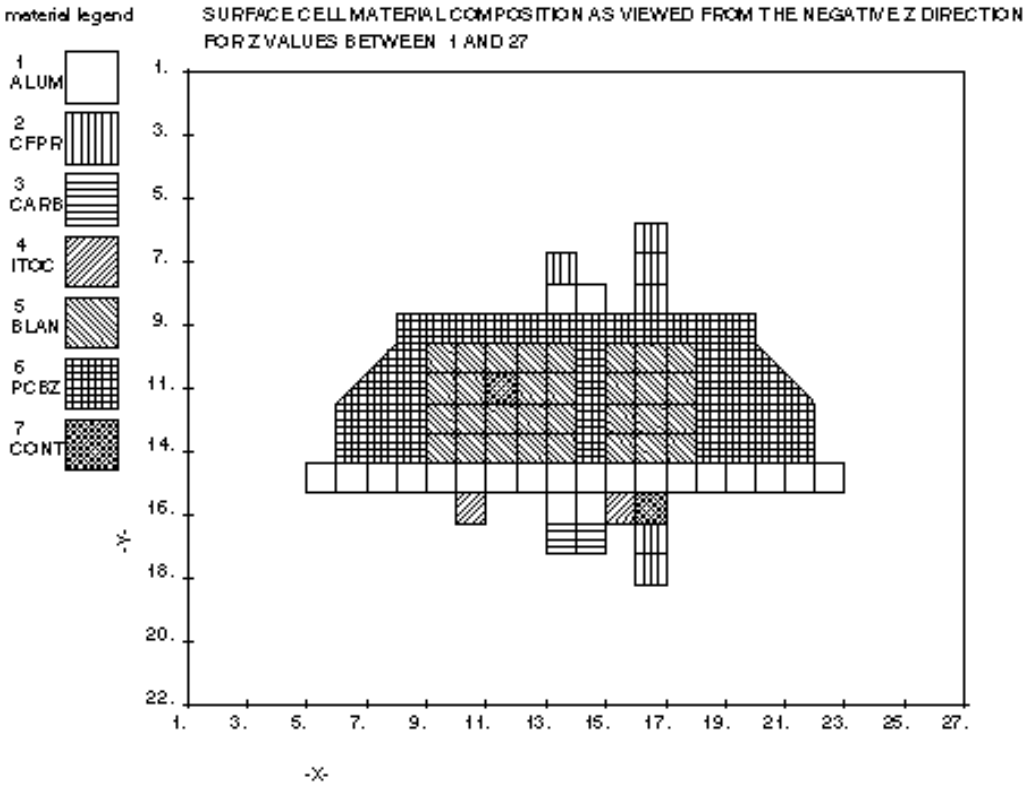

Figure 19. Distribution of materials on the -z side in model Cr.

4. MODELLING THE CHARGING ENVIRONMENT

The spacecraft-plasma interaction depends on the actual plasma parameters. The cold plasma density and temperature define the fundamental shielding properties of the plasma and the plasma currents to the spacecraft. We also need to know the ion composition, as the currents depend on particle dynamics. In auroral conditions, precipitating electrons are the important agents for charging, so we must also characterise the energetic electron environment. Additional information on sunlight/eclipse conditions and magnetic fields is also sometimes required, as is the orbital speed of the spacecraft.

For the simulations presented here we have, unless otherwise stated, assumed that the only ion species present is oxygen, and that ion and electron temperatures are equal. Including a component of hydrogen, which is likely to be present in reality, has the effect of decreasing the observed charging level as the lighter hydrogen is easier for the spacecraft to collect. The spacecraft speed is always put to 7 km/s, and the magnetic field is specified at its observed value and direction. However, the effect of satellite spinning is not included, so one particular spin phase value is picked at random (see also Section 5.1).

The precipitating auroral electrons are in POLAR modelled as a sum of a power law, a hot Maxwellian and a Gaussian population. If energy E and thermal energy KT are given in joules, the particle flux spectrum (unit: m^{-2} eV^{-1} $sr^{-1}s^{-1}$) can then be written as

$$\Phi(E) = AE^{-\alpha} + \frac{n}{\sqrt{2m_e}} \frac{E}{(\pi KT_2)^{3/2}} e^{-\frac{E}{KT_2}} + BE\, e^{-\frac{(E-E_0)^2}{\delta^2}} \qquad (6)$$

[PUM section 3.41] where A, α, n_2, T_2, B, E_0 and δ are free parameters that may be fitted to a measured distribution. The form of (6) is inspired by a statistical study of auroral zone electron spectra by Fontheim et al. [1982]. Although not perfectly flexible, we will see below that it actually can be used to get good fits to the electron spectra encountered by Freja in the events to be studied here (e.g. Figure 19). The distribution is mapped to a surface element on the spacecraft by use of energy conservation and Liouville's theorem, and the resulting current contribution is calculated by integration over energy. The Maxwellian and Gaussian components have analytic expressions for the integration over all energies, but for the power law component finite integration limits must be supplied since the integral diverges at zero energy.

One should note that in order to find the parameters in (6), we cannot directly compare to the electron spectra observed in the charging events. These refer to electron energy as measured at the spacecraft, which in charging events clearly will not be the same as the electron energy in the unperturbed plasma. We have therefore corrected for the observed charging level by mapping the POLAR flux expressions from the outside plasma in to the spacecraft by use of Liouville's theorem. This is done in the Matlab routines used for fitting of POLAR spectral parameters to observed spectra (Appendix K).

Expression (6) includes no reference to angular distribution, and POLAR assumes the distribution to be isotropic. In some situations the anisotropy of electron spectra may be an important factor for spacecraft charging processes, but this will mostly apply to spacecraft with large non-conductive parts. For Freja, the problem is expected to be small, because in the inverted-V electron events where charging is observed, the electron distributions are almost isotropic outside the loss cone. This is due to the isotropising effect of the magnetic mirror effect on particles travelling through increasing magnetic field magnitude when precipitating from the magnetosphere along the geomagnetic field lines down to the ionosphere.

Typical plasma conditions for the Freja charging events were discussed in WPs 110 and 130 [WP110, WP130]. For the simulations here we have also used additional detailed data. For determining the parameters describing the energetic electrons, we have visually fitted expressions of type (6) to electron spectra derived from observations by the TESP [Boehm et al., 1994] and/or MATE [Eliasson et al., 1994] electron detectors on Freja. For this study, the data was mainly available as hardcopies of plots, which were digitised using a slide ruler. The digitised data was plotted together with model spectra, as given by (6) but transformed to the energy levels and fluxes on the charged spacecraft as discussed above, in log-log-plots, and parameters were varied until reasonable fits were achieved. Plots of data and fits for each event are presented in Section 5.2. We do not put any strict definition of what is a "reasonable fit" here, but note that at the data points, the average discrepancy between data and models is below 15 per cent. Considering the uncertainties due to loss cones, material parameters and spacecraft models, this is not a critical problem, as is verified by the small variations of the final charging levels achieved for small variations of input environmental parameters (Section 5.2.7).

Plasma density is inferred from the identification of plasma oscillations and Langmuir waves, in wave data from the F4 instrument [Holback et al., 1994]. Observational Freja input on the electron and ion temperatures is weak, although T_e sometimes can be estimated from Langmuir probe sweeps of the F4 instrument if any reasonably interpretable sample is available close to a charging event. When no input is available, we assume 0.2 or 0.3 eV for ions and electrons alike.

5. SIMULATIONS OF CHARGING EVENTS

5.1 Event selection and characteristics

Out of the ten events studied in detail in this project [c.f. WP 110], five six-second periods (a full spin revolution) were selected for detailed simulation of the spacecraft charging process using SUCHGR and POLAR. Table 5 summarises the baseline environmental parameters, discussed in Section 4 above, used in the simulations.

Each event in Table 5 is studied during a full spin period, which is 6 seconds. In order to get reliable data from a presumably stable charging situation, not depending on for example the spin phase of the spacecraft or fast variations in the electron flux, we have chosen the six-second intervals to be modelled by looking for situations where the charging level, as given by the ion spectra [c.f. WP110], and electron spectra are as stable as possible over the six seconds. This implies that we do not necessarily model the highest charging levels found for each event in WP110. Initial studies of the spectra showed that the other alternative, namely picking the highest observed charging levels irrespective of stability of this level, would give very high uncertainties in environmental parameters and in the possible importance of dynamic effects on the charging. To test the predictive power of the charging codes, it is necessary to have as well-defined and stationary a situation as possible, while of course still have a significant charging level to model.

The plasma density on line 5 in Table 5 is therefore based on a plasma oscillation observed within these six seconds [c.f. WP110]. Electron and ion temperatures in lines 6 and 7 are assumptions, based on models [IRI-95] and Freja observations typical for this altitude range. Line 8 is the electron Debye length, line 9 the oxygen-based Mach number of the plasma flow seen in the spacecraft frame of reference, and line 10 is the assumed fraction of ions that are oxygen. The ion composition in the plasma is not well known, although 10 - 20 % protons and the remaining part O+ can be expected at this altitude. We have used 100 % oxygen in the simulations reported here as being a worst-case assumption, causing maximal charging levels (due to the higher inertial of heavier ions making them harder to attract to the spacecraft). We have to some extent tested the effect of varying the plasma parameters without finding any important differences, as discussed in Section 5.2.7.

Lines 11 to 19 in Table 5 are parameters defined by equation (6), based on visual fits of observed electron spectra (pcutl and pcuth are the integration cutoffs), as described in Section

4 above. Such fits are shown for each event below: for an example, see Figure 20. Lines 20 and 21 show magnitude and direction, in the spacecraft frame of reference, of the magnetic field as observed by the Freja F2 instrument [Freja magnetic field experiment team, 1994]. As the satellite is spinning around the y axis in our models and we consider spin averaged quantities, the direction of B in the x-z-plane is undefined. However, the angular relation between the directions of magnetic field, direction to sun (line 23) and plasma flow direction (line 24) are fixed, and we have arbitrarily chosen a spin phase angle such that the plasma flow is in the y-z-plane in all our simulations. Line 23 is the solar intensity, defined as 0 in darkness and 1 in full sunlight. An observed value of the spacecraft potential in this six-second interval, as based on ion data [WP110, WP130], is found on line 25.

1	Event #	3	6a	6b	7	9
2	Orbit	790	1666	1666	1785	736
3	Date [yymmdd]	921205	930209	930209	930218	921201
4	UT [hhmmss]	023828	091715	091800	093148	003508
5	n_e [cm^{-3}]	120	50	30	60	125
6	T_e [eV]	0.3	0.2	0.3	0.3	2
7	T_i [eV]	0.3	0.2	0.3	0.3	0.5
8	λ_D [m]	0.4	0.5	0.7	0.5	0.9
9	M_{O+}	5.2	6.4	5.2	5.2	4.0
10	n_{O+}/n_e	1	1	1	1	1
11	n_2 [m^{-3}]	1.5e3	2.2e5	6.2e5	5.2e4	1.3e5
12	T_2 [eV]	5e3	7e2	8e3	2.9e3	4e2
13	A [m^{-2} sr^{-1} s^{-1} eV^{-1}]	3.2e12	1.9e11	7.6e14	3e12	3.1e11
14	α	1.9	1.3	2.0	1.6	1.3
15	pcutl [eV]	0.5	0.5	0.5	0.5	0.5
16	pcuth [eV]	6.5e4	1e4	2e4	2e4	6e4
17	D [m^{-2} sr^{-1} s^{-1} eV^{-1}]	1.2e5	3e4	1.3e4	1.5e3	6e4
18	E_0 [eV]	1.5e3	2e3	1.1e4	1.3e4	1.8e3
19	δ [eV]	3e3	6e3	1.5e3	8.1e3	6.5e3
20	B [μT]	26	28	28	28	27
21	B direction (x,y,z) (model B)	0.1 -0.62 -0.78	0.55 -0.83 -0.02	0.55 -0.83 -0.02	0.76 -0.63 -0.19	0.71 -0.69 -0.14
22	Solar intensity	0	0	0	1	0
23	Sun direction (x,y,z) (model B)				0.12 -0.88 -0.46	
24	Flow direction (x,y,z) (model B)	0 -0.70 0.72	0 0.26 0.97	0 0.26 0.97	0 -0.21 0.98	0 -0.06 1.00
25	Observed potential [V]	-25	-40	-1000	-160	-40

Table 5. Freja charging event parameters for modelling by SUCHGR and POLAR. The table entries are described and discussed in the text in Section 5.1.

Event	3	6a	6b	7	9
Highest observed voltage (WP110)	-65	-1800	-1800	-500	-70
Observed voltage at modelled time	-25	-40	-1000	-160	-40
SUCHGR (ITOC)	-0.8	-0.1	-0.3	2.6	-0.6
SUCHGR (ALUM)	-7.2	-12	-72	2.9	-12
POLAR (model A)	-6.9	-5.4	-11	[-4..1]	-105
POLAR (model C)	-7.5	-4.1	[-40..0]	[-0.2..0.9]	

Table 6. Results of SUCHGR and POLAR simulations for the nominal environments defined in Table 5 above. Model A has 1 m grid size, model C grid size 10 cm. Table entries are potentials in volts. The bracket notation denotes that oscillations between the limits existed at the time of discontinuation of the simulation, but that it was clear that charging to observed level was not going to be reproduced even if the oscillations damped out.

5.2 Event simulations

After having defined the spacecraft model (Section 3) and the plasma model (Table 5), we have a well defined problem for the SUCHGR and POLAR codes. Simulations were run on three Sun workstations (Sparc-5, Sparc-20 and UltraSparc) running Solaris 2.5 and 2.6. In order to facilitate the reproduction of our results and the modification of inputs, we have included printouts of selected POLAR input files in Appendices B – G. Detailed instructions on how to run the POLAR software may be found in PUM. The files we reproduce here are fort.20 files for the VEHICL module of POLAR, defining the spacecraft model (Appendices C, D and E), and sample input files for the main module NTERAK (Appendices F and G). These files include the specification of the charging environment, as specified in Table 5, and computational settings for POLAR. To simplify for subsequent users of POLAR in general and these files in particular, the files are extensively commented, with references to applicable pages of PUM.

We have used the algorithms for space charge limited as well as and orbit limited current collection in these simulations. In a dense plasma, where the Debye length and sheath size are much smaller than the spacecraft dimensions, the space charge limited approximation will be

accurate, while the orbit limited approximation will fail because of too steep potential profile. In a tenuous plasma, where the Debye length is much larger than the spacecraft size, the orbit limited approximation applies, while the space charge limited assumption fails because there is no well defined sheath. POLAR is best suited to handle the space charge limited situation, as this can give a small sheath even in a charged situation. This will per definition not be true when we have charging in a situation where orbit limitation applies, as orbit limitation assumes slowly decaying electric field. POLAR uses a simulation grid of uniform grid size, making the simulation of a situation with an extended sheath practically incompatible with any detailed modelling of the spacecraft. When the code starts producing spacecraft charging to a level well below the thermal, the orbit limited assumption will be incompatible with the practical limitations of grid size. We therefore use the space charge limit as our nominal choice.

Table 6 summarises the results we get when using this direct approach on the problems. A detail of the charging sequence for one of the simulations (Event 6b, model A) is shown in Appendix J. Some of the table entries are based on orbit limited and some on space charge limited calculations, depending on the nature of the problem: for a detailed description of each simulation, please see Sections 5.2.1 – 5.2.5 below. The first line in Table 6 gives the maximum observed charging level for the event at hand. As noted in Section 5.1 above, this is not necessarily the voltage at the time we actually model, which is given in the second line in the table. It is evident from Table 6 that our straightforward modelling using available measurements and knowledge of the satellite in no case reproduces the observed charging levels. Possible reasons for this behaviour are discussed in Sections 5.2.7 and 5.3.

The actual running of the POLAR code in these simulations is discussed briefly in Appendix J. Two input files for the NTERAK module of POLAR, which is the routine actually doing the calculations, are listed in Appendices F (for event 3 using model C) and G (for event 6a using model A). All simulations are completely documented, with all input and output files used in the simulations, on the simulation file tree that has been delivered to ESTEC on CD-ROM (see also Appendix H).

5.2.1 Event 3, 921205 02:38, charging at sunset during auroral substorm.

Parameters for this event are summarised in Table 5. Figure 20 shows the electron spectrum as obtained by the TESP and MATE detectors, which both were operational in this event. The parameter fit in Figure 20 is made to the data with no correction for the spacecraft

charging level changing the zero reference of the energy scale. Such a correction, implemented as described in Section 5.1 above, leads to the fit in Figure 21. Note that the data are the same in both cases, but when doing the fit in Figure 21, the flux expression (6) assumed by POLAR is mapped to detector energy levels using Liouville's theorem. We simulate using both sets of parameters, to show the effect of the energy correction in this low-level charging event.

In WP110, it was shown that the maximum charging level during this event reaches levels up to almost -65 V. The six-second interval we have chosen for detailed study here shows charging to -25 V. As discussed in Section 5.1, the reason for choosing this particular interval rather than the time of highest charging level is that we want the charging level be stable for the six seconds required to get a full pitch angle coverage, so that the use of spin-averaged electron data is justified. Such a stable situation was found between UT 023825 and 023831.

To model this charging event, we have run nine POLAR simulations, the results of which are shown in Table 7. The best-effort direct simulations using models Ar and Cr yields -6.9 V and -7.5 V, respectively. The equipotential contours in the x-y-plane around the spacecraft for these simulations are shown in Figures 22 and 23.

All event 3 simulations converge to final resulting spacecraft potentials. In this case, the final result seems independent of the initial voltage. That this is no general truth is discussed in Section 5.2.7. It is hard to say something conclusive on the difference between models with different material properties: 3:3 and 3:4 give rather similar results, while 3:7 and 3:8 differ by a factor of two. However, the importance of correcting the electron spectra for the potential difference between the spacecraft-mounted detector and free space is well demonstrated, as the runs with corrected spectra show significantly more charging than the others.

Figure 22 shows that the quality of the simulation 3:5 is good in the sense that the sheath edge stays well away from the simulation box edge, at the same time as the sheath size is several grid units in width. Should any of these conditions be violated, the reliability of the result will decrease. If the sheath reaches close to the edge, the boundary condition on potential used by POLAR (zero potential at one grid unit outside the simulation box) will affect the value of the calculated potential. On the other hand, if the sheath comes closer to the spacecraft than a grid unit, the fields in the sheath can obviously not be accurately modelled.

Simulation #	Collection	S/C model	Initial V	Spectra	Comments	Result
3:1	orblim	Am	-25	raw		-2.4
3:2	orblim	Am	-25	corr		-6.6
3:3	spclim	Am	-25	raw		-2.9
3:4	spclim	Ar	float	raw		-3.4
3:5 *	**spclim**	**Ar**	**float**	**corr**		**-6.9**
3:6	orblim	Cn	float	raw		-1.2
3:7	spclim	Cn	float	raw		-3.4
3:8	spclim	Cp	float	raw		-1.6
3:9 *	**spclim**	**Cr**	**float**	**corr**		**-7.5**

Table 7. POLAR simulations performed on Freja charging event 3. Column descriptions: *Simulation #*. Stars * indicate nominal best-effort simulations. *Collection.* Orbit or space charge (sheath) limited approximations. *S/C model*. See Table 4 for explanation. *Initial V*. Initial potential in volts, "float" means that the POLAR default floating potential is used. *Spectra*. Tells whether or not correction for observed charging has been made. *Result*. Final resulting bulk potential of the spacecraft, in volts.

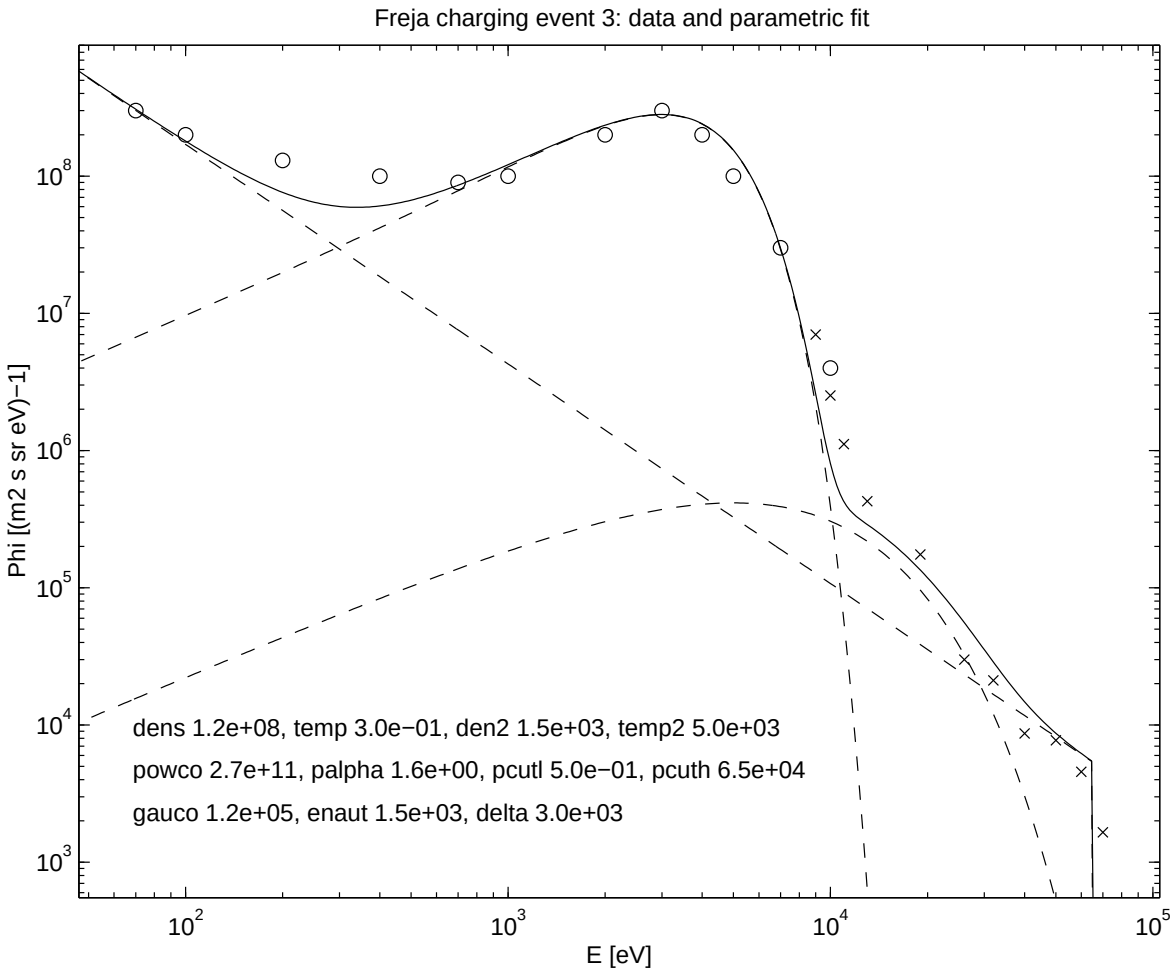

Figure 20. TESP (o) and MATE (x) electron data for event 3, together with a fit to expression (6) with parameters as printed. The fitted curve does not take the observed charging level into account. Dashed lines show the contribution from the individual electron populations recognised by POLAR: hot Maxwellian, power law, Gaussian.

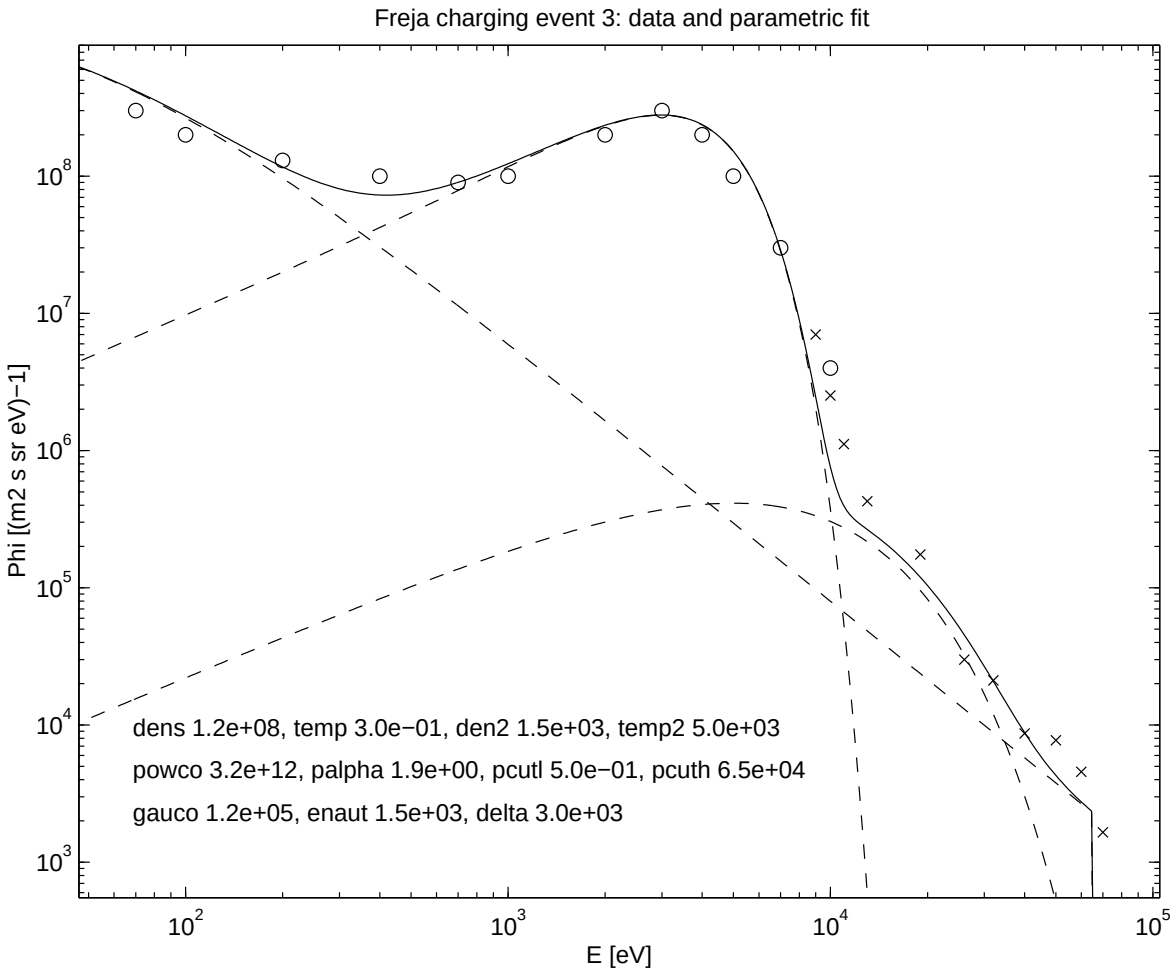

Figure 21. TESP (o) and MATE (x) electron data for event 3, together with a fit to expression (6) with parameters as printed. The fitted curve is corrected for the observed charging to -25 V.

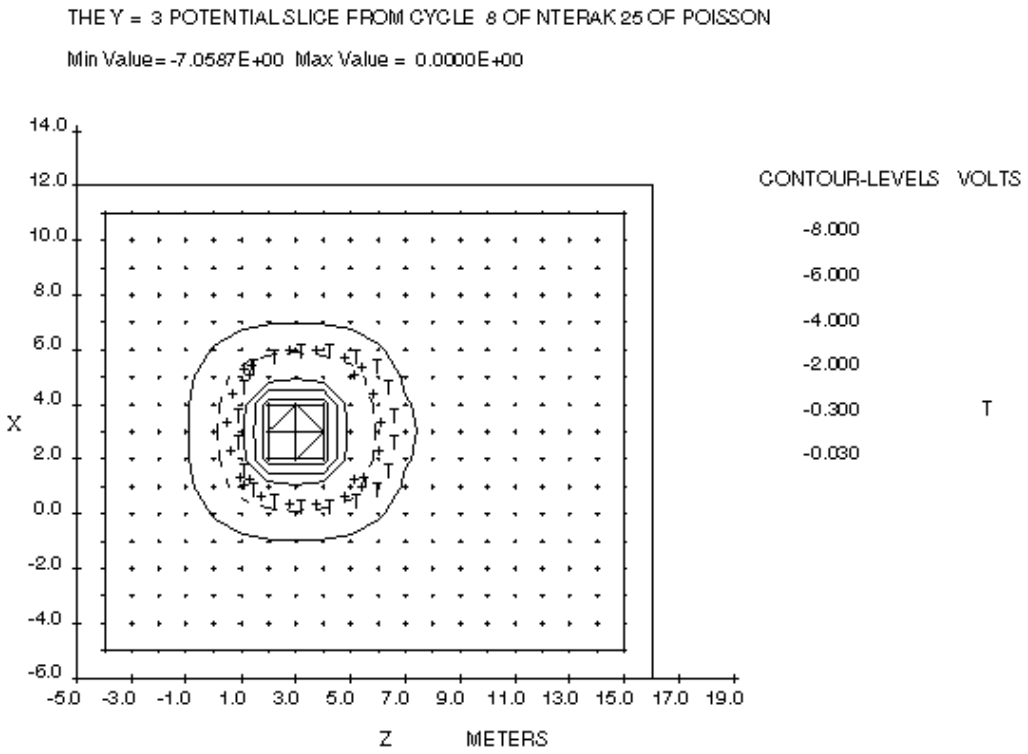

Figure 22. Equipotential contours in the x-y-plane for the nominal model Ar simulation. The solid contour is the sheath limit, as defined in Section 2.3 (i.e., by $|\Phi| = 0.47\, KT_e / e$). The contour marked by 'T' denotes $\Phi = -K\,T$. Other contours are separated by 2 V. It can be seen that the sheath stays well away from the boundaries, while still being several grid units thick.

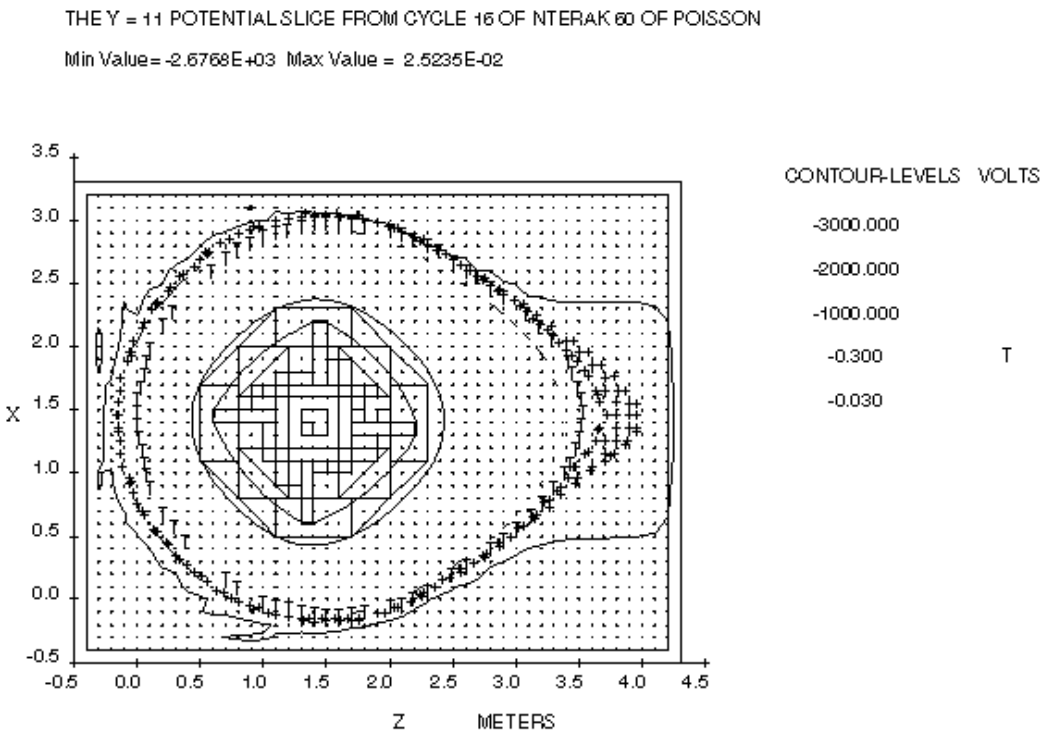

Figure 23. Equipotential contours for simulation 3:9. For explanations, see Figure 22.

5.2.2 Event 6a, 930209 09:17, beginning of an intense auroral inverted-V event

The charging environment is shown in Figure 24, simulation results in Table 8 and equipotential contours for the nominal simulations in Figures 25 and 26. It can be seen that while the nominal simulations does not reproduce the observed charging level, changing the initial condition gives a value very close to the observed (simulation 6a:1). Figure 25 shows that the boundary condition at the simulation box edge may play a role, so the -38 V result of 6a:1 may partly be a coincidence. However, more interesting than the exact level of charging reproduced in the simulation is perhaps the fact that some charging at all is predicted. This cannot be due to the boundary condition. Instead, it shows us the importance of the history of the charging process, as is further discussed in Section 5.2.7.

Other simulations (6a:3, 6a:4) also predict significant charging, but as they are based on uncorrected data, their prediction does not mean anything. However, we may note that the

orbit limited calculations (6a:3, 6a:6) predicts more charging than does corresponding space charge limited simulations (6a:4, 6a:7).

The problem with finite simulation box is more pronounced for model C than for model A. Figure 26 shows that the sheath reaches the simulation box boundary already at the modest charging level of -4.1 V calculated in this case.

Simulation #	Collection	S/C model	Initial V	Spectra	Comments	Result
6a:1	spclim	Ar	-40	corr		-38
6a:2 *	**spclim**	**Ar**	**float**	**corr**		**-5.4**
6a:3	orblim	Am	-40	raw		-55
6a:4	spclim	Am	-40	raw		-29
6a:5 *	**spclim**	**Cr**	**float**	**corr**		**-4.1**
6a:6	orblim	Cn	float	raw		-18
6a:7	spclim	Cn	float	raw		-15

Table 8. POLAR simulations performed on Freja charging event 6a. For explanations, see Table 7. Parameters for raw spectra: den2 = 2e5, temp2 = 6e2, powco = 6e10, palpha = 1.3, pcutl = 0.5, pcuth = 1e4, gauco = 3e4, enaut = 2e3, delta = 6e3.

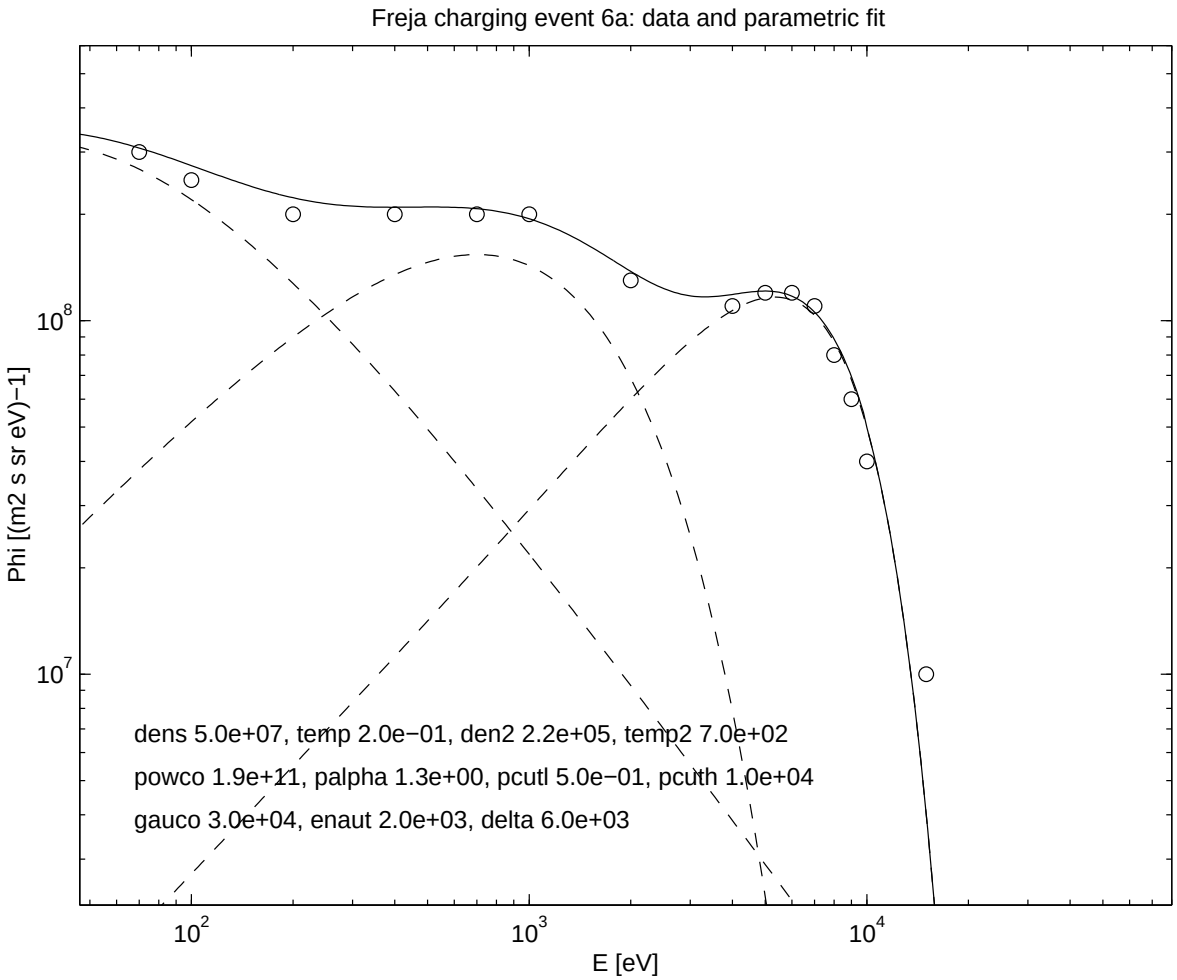

Figure 24. TESP electron data for event 6a, together with a fit to expression (6) with parameters as printed. The fitted curve is corrected for the observed charging to -40 V.

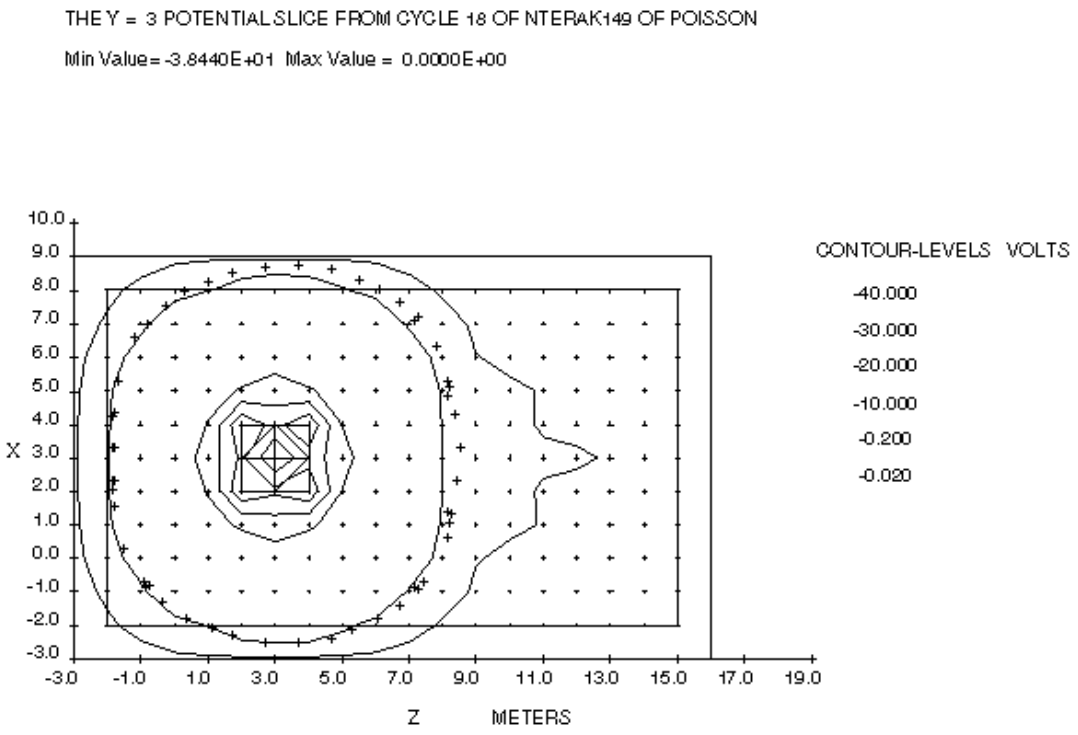

Figure 25. Equipotential contours for simulation 6a:1. For explanations, see Figure 22.

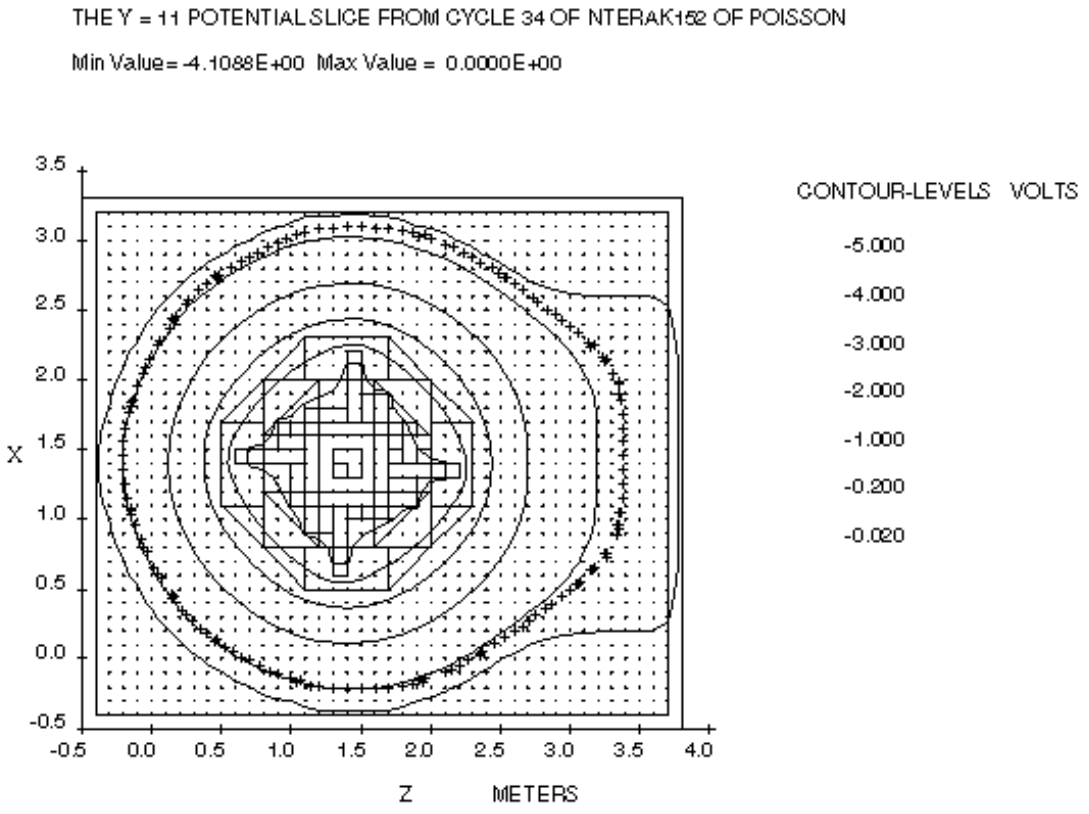

Figure 26. Equipotential contours for simulation 6a:5. For explanations, see Figure 22.

5.2.3 Event 6b, 930209 09:18, peak of an intense auroral inverted-V event.

This is the most pronounced charging event in this study, reaching down to -1000 V. Close to the six-second interval chosen for the simulations, still lower potentials (-2000 V) are observed [WP 110]. Electron data and (corrected) fit are showed in Figure 27. Comparing to Figure 24, which shows data taken 45 seconds earlier, the pronounced peak around 1 keV (detector energy level) is obvious. Simulation results are displayed in Table 9. In this case, we did not do as in events 3 and 6a, where we were using uncorrected spectra to find the effect of parameter variation. The charging potential is here so high that uncorrected spectra will be very different. Instead, we use a variation of the uncorrected spectra from event 6a, with a much increased temperature of the hot Maxwellian and high peak energy for the Gaussian. This defines a "var" environment, whose parameters are given in the caption to Table 9.

Table 9 shows that the nominal simulations do not reproduce the observed charging levels. One of them (6b:4) did not converge to a final result before the simulation was stopped, but before starting to oscillate it raised monotonically from -800 V to -40 V, so it is clear that no charging to observed levels would ever have appeared in this run. Figure 29 shows that the sheath reaches the simulation box edge only in the wake. For model A, Figure 28 tells us that there was little problem with the finite simulation box in this case, and the -11 V result should thus be a good value in this respect.

Charging is actually predicted in several of the simulations running the modified "var" environment. Simulations 6b:2, 6b:7, 6b:8 and 6b:9 all showed steadily decreasing potentials, showing no signs of reaching a final value when the runs were discontinued. It is to be noted that for these simulations, the boundary condition on potential at the simulation box edge will have an enormous impact. In reality, the sheath edge, as defined by default in POLAR (see Section 2.3) may expand to hundreds and even thousands of spacecraft radii if charging to a level of 10,000 times *KT/e* occurs in a tenuous plasma, as is the case here. Therefore, we do not expect correct reproduction of observed values in this case, except if a sheath fitting into the simulation box had been found, which is not the case. However, we have an indication of strong charging, even if we cannot trust the quantitative results. Thus, strong charging actually can be qualitatively predicted by POLAR, but of course the spectrum "var" we used here is not correct ("corr"). Comparing 6b:2 and 6b:3, we see that the choice of model here plays an important role. If OML theory is used, charging is attained, while the sheath limit gives no charging.

Simulation #	Collection	S/C model	Initial V	Spectra	Comments	Result
6b:1 *	**spclim**	**Ar**	**float**	**corr**		**-11**
6b:2	orblim	Ar	float	var	Sheath expansion	(< -3180)
6b:3	spclim	Ar	float	var		-8.1
6b:4 *	**spclim**	**Cr**	**-800**	**corr**	**Rising steadily to -40 V, then oscillating**	**(-40** — 0)
6b:5	orblim	Cr	float	corr	Oscillating	(-60 — 0)
6b:6	orblim	Cr	float	var		-27
6b:7	spclim	Cn	float	var	Sheath expansion	(< -2120)
6b:8	spclim	Cp	float	var	Sheath expansion	(< -2800)
6b:9	spclim	Cp	float	var	Sheath expansion, sthpot set	(< -6290)

Table 9. POLAR simulations performed on Freja charging event 6b. For explanations, see Table 7 and text. Parameters for var spectra: den2 = 2.6e5, temp2 = 4.3e3, powco = 6e10, palpha = 1.3, pcutl = 0.5, pcuth = 1e4, gauco = 2.5e4, enaut = 1.1e4, delta = 3.4e3.

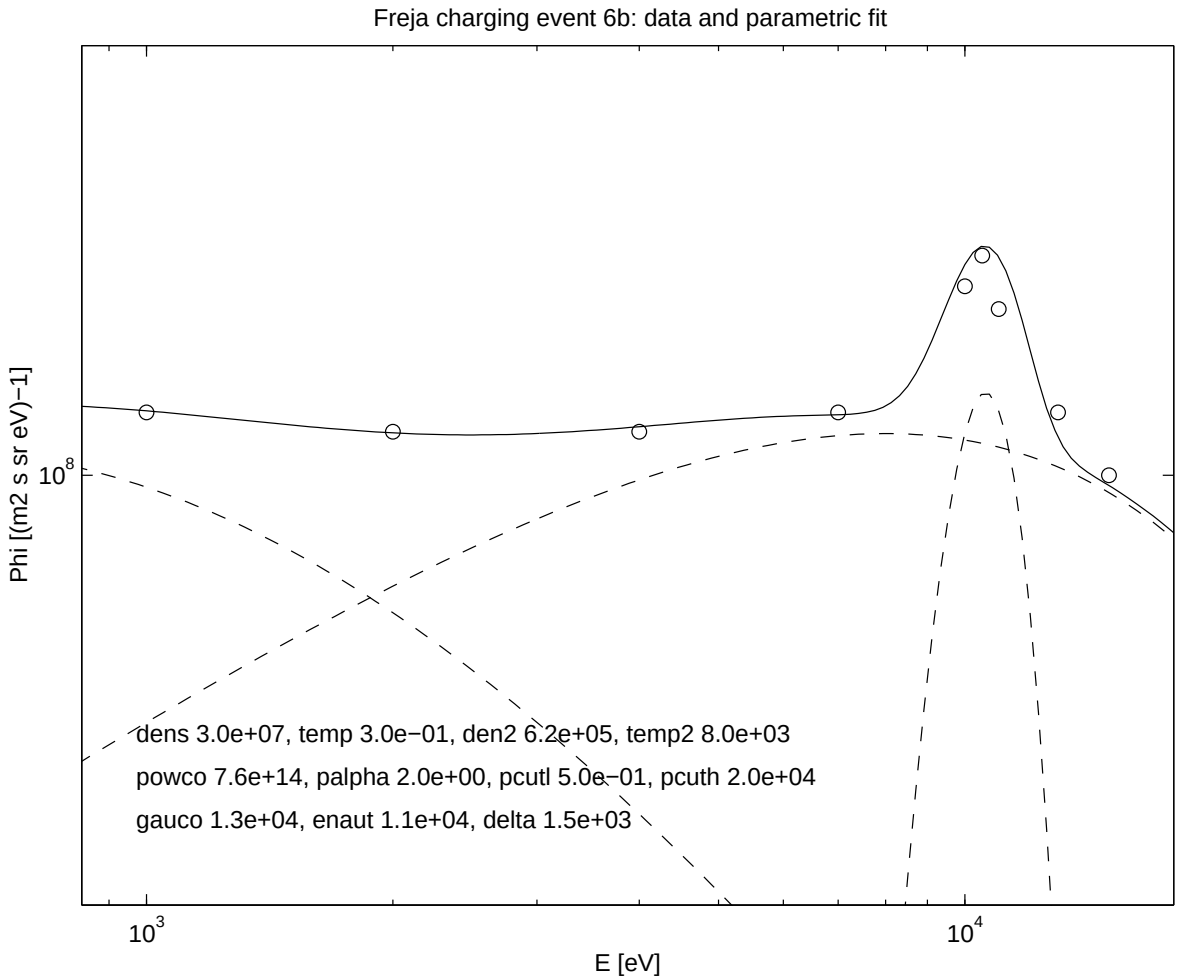

Figure 27. TESP electron data for event 6b, together with a fit to expression (6) with parameters as printed. The fitted curve is corrected for the observed charging to -1000 V.

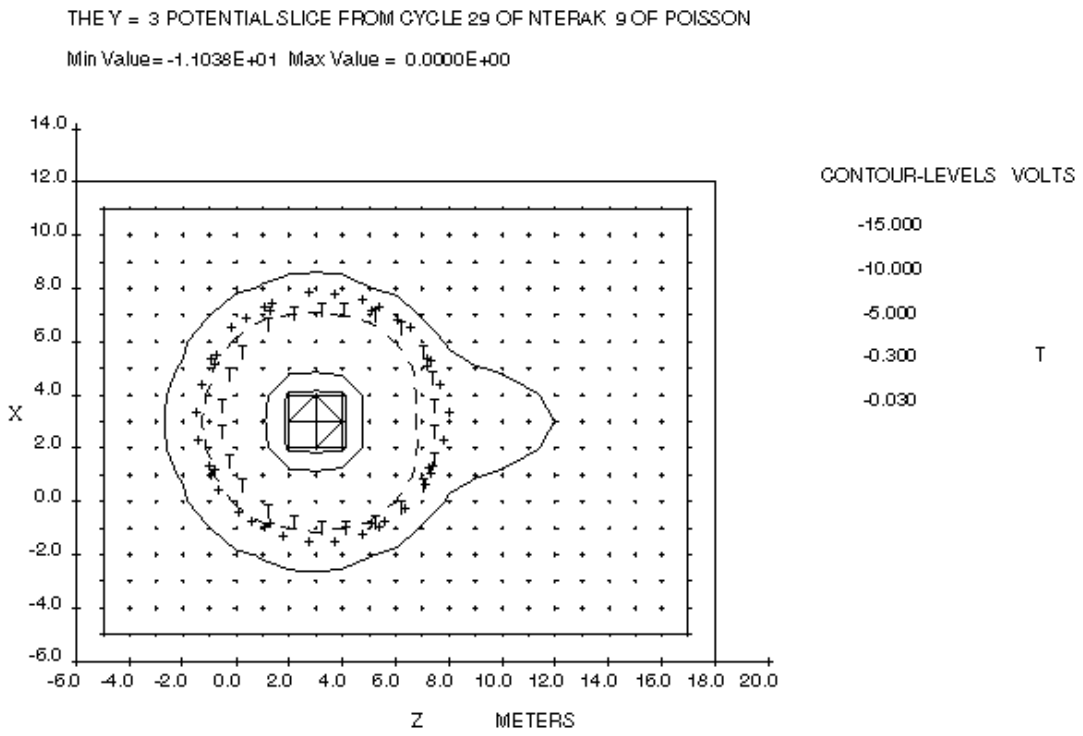

Figure 28. Equipotential contours for simulation 6b:1. For explanations, see Figure 22.

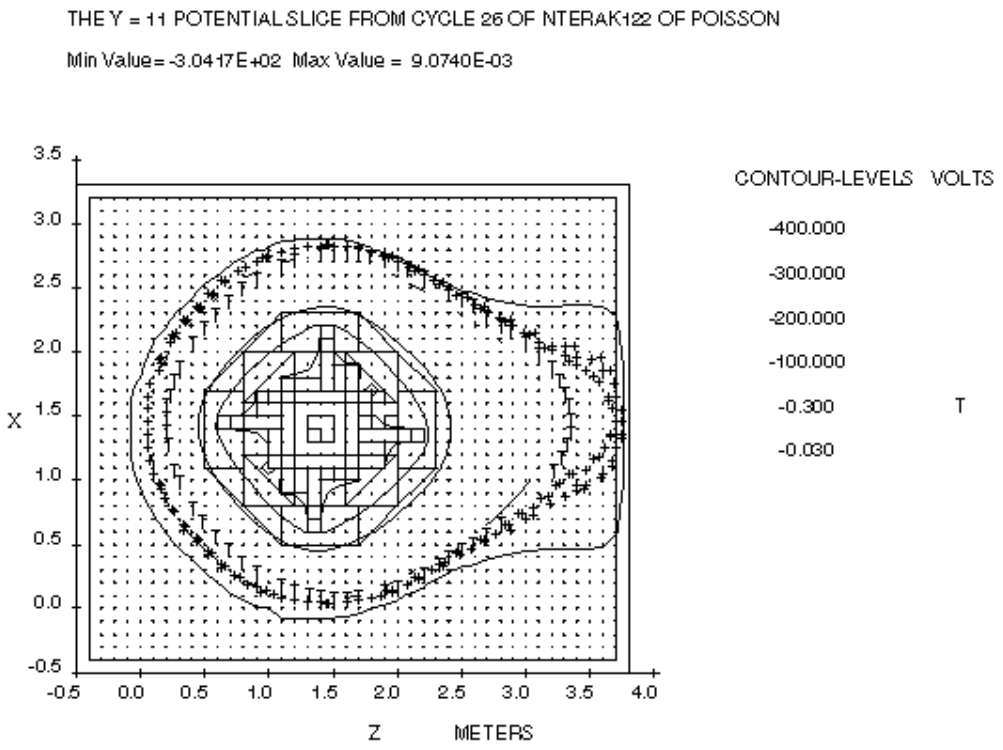

Figure 29. Equipotential contours for simulation 6b:4. For explanations, see Figure 22.

5.2.4 Event 7, 930218 09:32, sunlight conditions during auroral inverted-V event.

Electron data for this event are shown in Figure 30, and simulation results in Table 10. No simulation presents any result remotely like the observed charging level, irrespective of material properties, charging environment used or initial conditions. The best is 7:2, which uses model Am, in which all secondary and photoelectron yields have been arbitrarily decreased to two thirds of their nominal values, but even this is not sufficient to bring about the observed charging.

Simulation #	Collection	S/C model	Initial V	Spectra	Comments	Result
7:1 *	**spclim**	**Ar**	**-50**	**corr**	**Steady rise to -5 V, then osc.**	**(-4 — 1)**
7:2	spclim	Am	-50	corr		-5.7
7:3	orblim	Am	-50	raw		-2.6
7:4	spclim	Am	-50	raw		-1.6
7:5 *	**spclim**	**Cr**	**-50**	**corr**	**Steady rise to -1 V, then osc.**	**(-0.2 < V < 0.9)**
7:6	orblim	Cn	float	corr	Oscillating	(-1 < V < 2)
7:7	orblim	Cn	float	raw		+1.0
7:8	spclim	Cn	float	raw	Still rising	> 0

Table 10. POLAR simulations performed on Freja charging event 7. For explanations, see Table 7. Parameters for raw spectra: den2 = 4.7e4, temp2 = 2e3, powco = 3.4e10, palpha = 1.05, pcutl = 0.5, pcuth = 2e4, gauco = 1.7e3, enaut = 8.2e3, delta = 1.3e4.

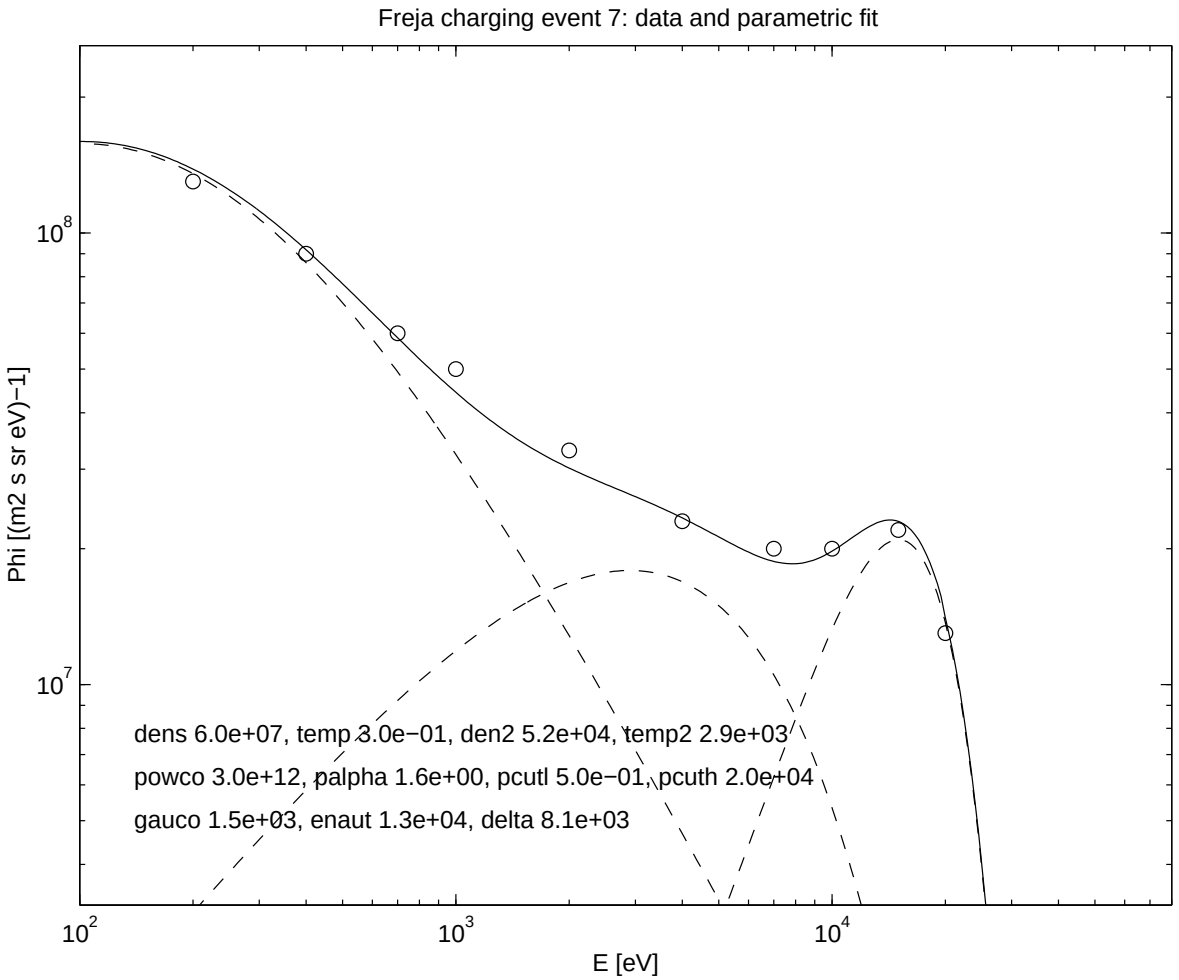

Figure 30. TESP electron data for event 7, together with a fit to expression (6) with parameters as printed. The fitted curve is corrected for the observed charging to -160 V.

5.2.5 Event 9, 921201 00:35, charging during variation of plasma density.

Data and fit for this event can be seen in Figure 31. Table 11 summarises the results, and equipotentials for the nominal simulation 9:1 are shown in Figure 32.

In this case, the nominal simulation actually predicts even stronger charging than observed. Figure 32 shows that the simulation result is not strongly affected by boundary conditions. The importance of correcting the electron flux expression for the observed charging is obvious in this case as well, as the other simulations do not show much charging irrespective of detailed material parameters. The fact that the charging that is predicted is too strong is not

so bad, considering the very low spatial resolution of the Freja model A used here, with correspondingly poor accuracy in the surface areas of different materials.

Simulation #	Collection	S/C model	Initial V	Spectra	Comments	Result
9:1 *	**spclim**	**Ar**	**-40**	**corr**		**-105**
9:2	orblim	Am	-40	raw		-4.2
9:3	spclim	Am	-40	raw		-4.4
9:4	orblim	Cn	float	raw		-0.9
9:5	spclim	Cn	float	raw		-1.0

Table 11. POLAR simulations performed on Freja charging event 9. For explanations, see Table 7. Parameters for raw spectra: den2 = 1.3e4, temp2 = 8.5e3, powco = 4.3e9, palpha = 0.5, pcutl = 0.5, pcuth = 1e4, gauco = 3.5e4, enaut = 4e3, delta = 5e3.

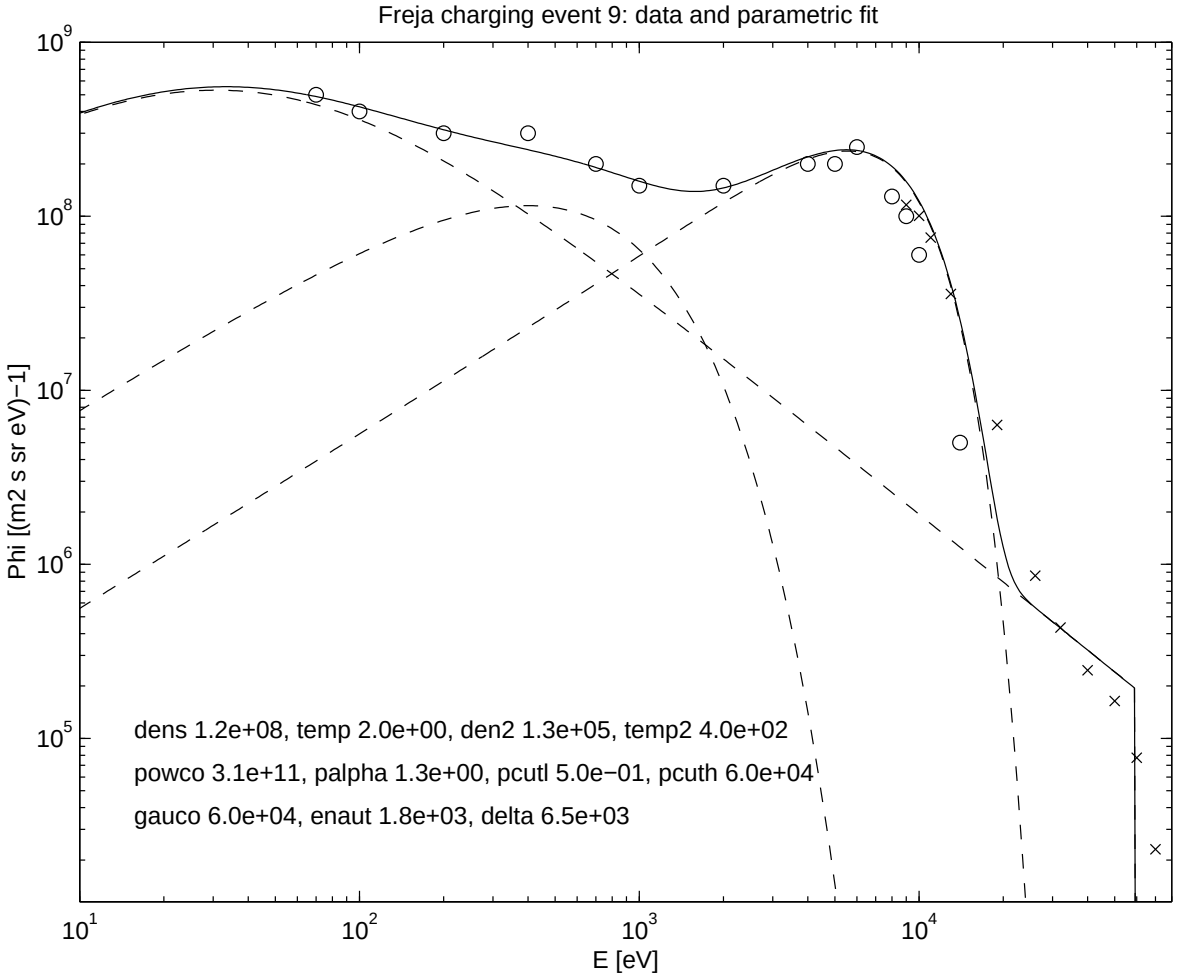

Figure 31. TESP electron data for event 9, together with a fit to expression (6) with parameters as printed. The fitted curve is corrected for the observed charging to -40 V.

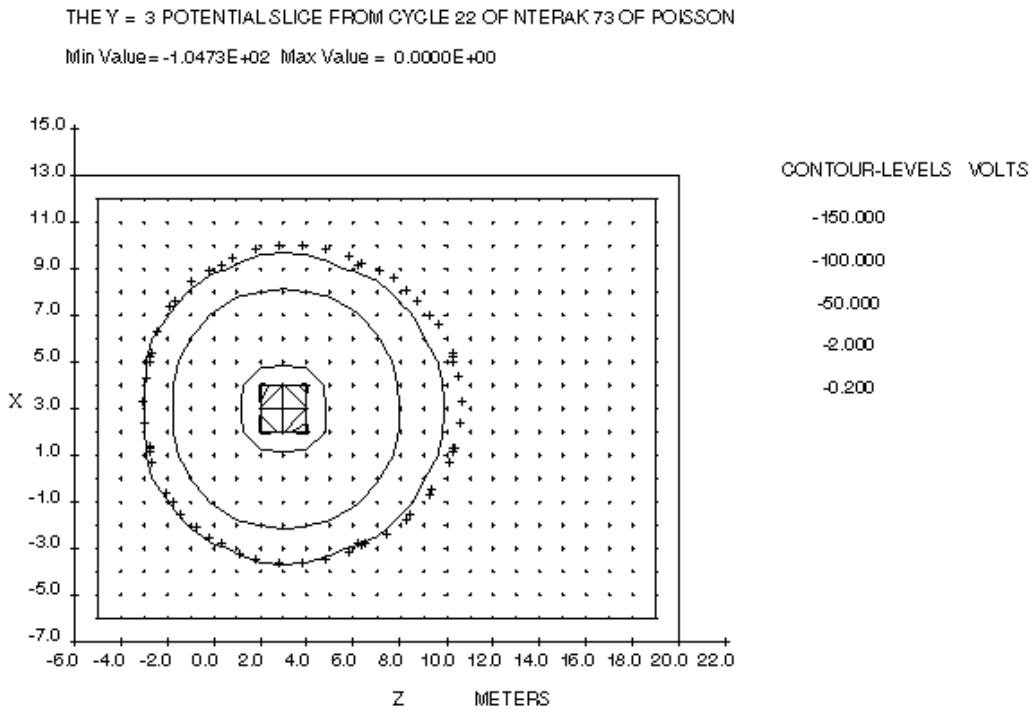

Figure 32. Equipotential contours for simulation 9:1. For explanations, see Figure 22.

5.2.6 "Event D": Comparison Freja-DMSP charging

To compare this Freja charging study to other work using the POLAR code, it is instructive to see how our Freja model behaves in a charging environment studied for the DMSP satellite. The POLAR 1.3.7 code distribution includes a model of DMSP as well as a plasma environment in the directory pol1.3.7/run/dmspwe, which when run yields a charging of -195 V. We have run Freja model Ar using the same input to NTERAK, which resulted in charging to a level of -40 V (Table X). This lower level of charging is consistent with the general observation of WP110 and WP130: due to its smaller areas of non-conducting material, Freja is more resistant to charging than is DMSP.

Simulation #	Collection	S/C model	Initial V	Spectra	Comments	Result
D:1	spclim	Ar	float			-40
D:2	spclim	DMSP	float			-195

Table 12. POLAR simulations performed on Freja and DMSP for the DMSP environment specified in the POLAR 1.3.7 distribution. For explanations, see Table 7.

5.2.7 Variations of environment parameters

Most of the Freja charging events are strongly associated with high-energy electrons during auroral inverted-V events, as shown in WP 130. Therefore these hot plasma parameters are quite crucial, and were therefore investigated to show how variations of these affect the simulation results. Small variations of the other environment parameters did not give any significant changes in the results. These were therefore held constant during the simulations varying the hot electron temperature and the hot electron density. To simulate combined variations of all the environment parameters cannot be within the scope of this study as the number of combinations is enormous.

Values from event 6b were used because of the great charging level observed. We used not the nominal environment as given in Table 5, as this did not cause any significant charging levels. Instead we used the "var" environment specified in the caption to Table 9, and varied its parameters. It was found that a change of den2 from 2.6e5 m^{-3} to 2.0e5 m^{-3} decreases the voltage from -8.1 V to -26.6 V, and that we get -82.1 V for a den2 value of 1.5e5 m^{-3}. A change of temp2 from 0.43e4 eV to 1.0e4 eV lowers the voltage from -8.1 V to -151 V. The two parameters were varied over a wide range to see if and what values could give rise to the observed voltage of -1000 V in event 6b. The results are presented in Figure 33.

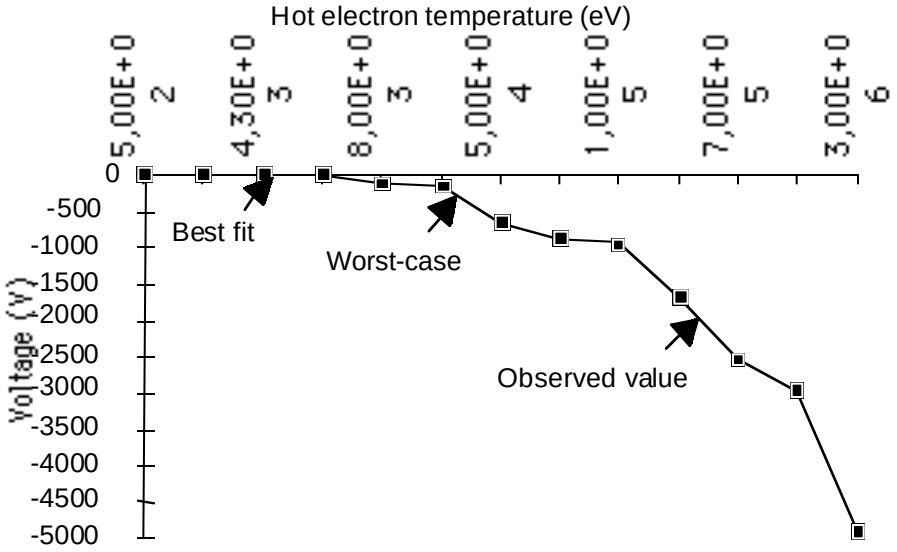

Figure 33. Results from POLAR simulations varying the hot electron temperature. The rest of the environment parameters are from the "var" environment in Table 9. Model Ap is used.

Increasing the temperature can give the level of charging observed by Freja but these values are far out of range from the measured values and making fits with these values does not correspond well. To get a charging of -1000 V, a hot Maxwellian temperature (temp2) of about 1e5 eV is needed.

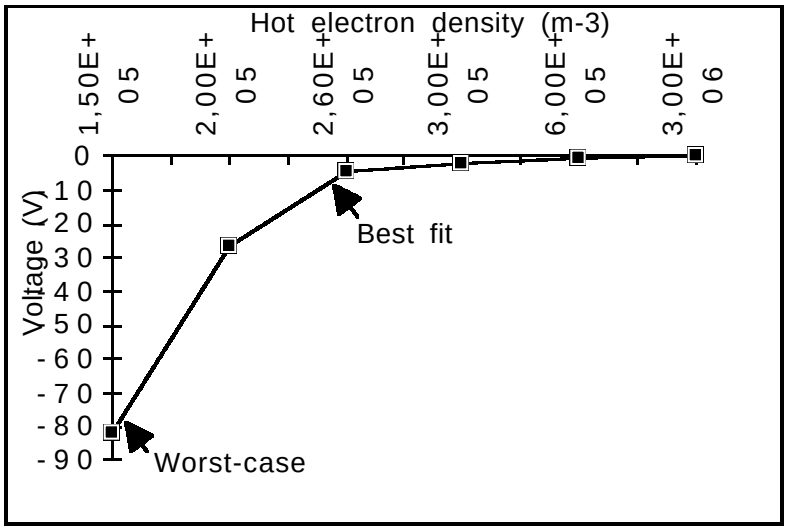

Figure 34. Results from POLAR simulations varying the hot electron density. The rest of the environment parameters are from the "var" environment in Table 9. Model Ap is used.

Decreasing the hot plasma density (den2) just a little bit lowers the voltage significantly but does never come close to the observed level of -2000 V. A lower level than -213 V is not reached bringing the density down to zero.

It is thus possible to get reasonably good fits with the electron spectra using quite extreme values of the hot electron temperature. As a worst-case value, we have used 10 keV. The lowest voltage as function of hot electron density seems to be reached setting the density equal to zero. This would mean that there would be no hot electrons at all, making the influence of hot electron temperature zero as well. Instead we use a density of 1.5e5 as a worst-case value.

The worst-case parameters give a simulation result of a charging level of -177 V, quite different from the best-fit value of -8.1 but it is important to remember that these parameter values are highly improbable in accordance with the observed data. Even with these extreme values, the simulated -177 V is still far from close to the observed -2000 V implying that uncertainties in these parameters only can account for a small part of the discrepancy between the code simulations and the observations.

It is possible to find multiple solutions to the simulations by starting at different initial voltages of the spacecraft, as discussed in Section 2.5 and seen above in Section 5.2.2. The simulations we have done have used instantaneous values of the plasma parameters, and most often we assume the floating potential as initial condition. A realistic simulation may need to proceed in steps tracking the history of the plasma and the charging.

Initial voltage (V)	Final simulated voltage (V)
0	-4.2
Float	-8.1
-80	-78.1
-400	-398
-900	-897

Table 13. POLAR simulation results varying the initial voltage on model A, event 6b, environment "var".

5.3 Discussion of the simulation results

Section 5.2 revealed that we very rarely achieved the observed levels of charging in the simulations. If sticking to the observed parameters for energetic electrons and starting the calculation from floating potential, in fact only one simulation (9:1) gave a result close to observations. There are several possible sources for the observed discrepancy between the observed charging voltages and the POLAR predictions. They may be grouped into (a) errors in the spacecraft definition, (b) errors in the plasma environment definition, (c) errors in the application of the code and (d) limitations of models used in the code. A fifth possibility, namely pure software bugs, is considered less likely as POLAR has been extensively tested for other situations and showed to work there [Katz et al., 1989b]. We discuss each of these possibilities below.

(a) *Spacecraft definition.* For all the major materials on Freja, we have used parameters established in the laboratory. The exception are the relatively small areas of the nozzles and TM antennas, for which we have assumed material parameters as for CFRP but with very low conductivity, and the also small aluminium parts, for which we have used unoxidized aluminium as model. However, defining the carbon fibre areas as CONT or CFRP has been found to make no big effect to the simulations, and the use of pure aluminium parameters should exaggerate rather than diminish the predicted charging level as the secondary electron yield increases in the oxidisation process. If something should be wrong in the material description it must be for some of the more dominating Freja surface materials. One may note that Freja charging events are seen from the very beginning of the mission, so material ageing is a less likely cause of the discrepancy. It is outside the scope of this study to experimentally investigate the properties of the materials used. As an example one may note that if the assumed high conductivity of the PCB-Z paint should be significantly lower than thought, this would bring a major change to the spacecraft model, making a major part of the spacecraft an effective dielectric. Another such possibility is that the ITO cover on the thermal blankets may crack and decrease in conductivity. Such effects could cause the build-up of large differential charging levels, which by influencing the potential distribution in the plasma and hence the particle orbits may cause an overall charging of the spacecraft.

Spacecraft model problems could also be in the geometry of the spacecraft. An even more detailed model of the spacecraft may possibly give better results. We think this is less likely, as it all major parts are quite accurately modelled by model C above (Section 3.3). Although we do not think it likely, it is in principle possible that some of the larger linear elements on

Freja, like the magnetometer booms, could influence the potential distribution and thereby change the charging level. One further study could thus be to construct a Freja model for NASCAP, which can handle booms. Although NASCAP cannot accurately model the auroral spectra seen by Freja, a comparison between NASCAP and POLAR results for a charging environment they both can handle could be of interest.

(b) *Plasma environment*. Several of the plasma parameter values we have used are rather uncertain. For the cold plasma, the temperatures we have used are assumed values. However, varying these within reasonable limits does not very much change the voltage predicted by POLAR. Taking event 3 as an example, runs on model C with temperature 0.1 eV and 1 eV yields spacecraft potentials of -1.3 V and -3.8 V, respectively, which is not dramatically different from the -1.2 V observed for the nominal parameters. We do not think the cold plasma density could be a major source of error. First, the density values in these charging events are already very low for this altitude range. Second, our identification of the narrowband HF emissions on which we base our density estimates as plasma oscillations and Langmuir waves [WP110] has been verified by comparison of these emissions with the Langmuir probe current in non-charging events. Third, the ion spectra in the charging events show an uplift in energy of the ram flow, not a major decrease of the ram flow intensity, which should be the case if the density dropped drastically.

The high-energy electrons are well measured by the TESP and MATE detectors, who have proved their values in numerous studies [e.g., Boehm et al., 1994; Eliasson et al., 1994]. In the region of overlapping energy, the two detectors give very similar shapes of spectra, and spectra well within a factor of two from each other. However, we should note a few possibly important uncertainties. First, in the events studied, no truly field-aligned electron spectra have been obtained. The pitch-angle coverage of the detectors depended on the spacecraft attitude. The perpendicular direction is always covered, but pitch angles below 20^o was not covered in any of our cases. Table 14 summarises the pitch angles of the spectra used, and the observed anisotropies. In some cases, there is no sign of anisotropy in the pitch angle range covered (events 7 and 9), while others may show such anisotropies, in particular for the energy range around 1 keV, which has important impact on the secondary electron production. For the modelling, the 90^o spectra have been given more attention, as in an averaging process to find the omnidirectional flux, the directional fluxes will be weighted by the sine of the pitch angle. However, we should note that there in principle might be energetic electrons at near-parallel or near-antiparallel pitch angles, which we do not measure. As we do not know anything about such electrons, and POLAR includes no mechanism to model

them even if we had knowledge of them, their hypothetical impact is impossible to assess. An extended study could search for Freja charging events with better pitch angle coverage, or use another data set with more complete pitch angle coverage most of the time. Even so, the only way to include them in a POLAR 1.3.7 simulation would be to use pitch-angle averaged spectra.

Event	**Available P/A** [^{o}]	**Anisotropy**	**Used P/A** [^{o}]
3	68, 69, 84, 100	Peak value (3 keV) factor 2 higher at 68^o than at 90^o.	68
6a	33, 34, 90, 103	Peak value slightly higher at 90^o. Flux at 1 keV factor 4 higher at 90^o and 103^o than at 33^o and 34^o.	90
6b	32, 33, 90, 104	Peak isotropic. Factor 2 higher flux at 1 keV at 90^o and 104^o than at 32^o and 33^o.	Average
7	22, 23, 90, 103	Isotropic	-
9	44, 46, 88, 93	Isotropic	-

Table 14. Observed anisotropies in the spectra used for the specification of the nominal electron environments for the modelled charging events. All energies are as observed at the detector, which in charging events will be different from the particle energy in the unperturbed plasma.

(c) *Application of POLAR*. The POLAR code is a complex numerical package with several options on the use of physical and numerical models and of numerical parameters. A straightforward application of the default settings of the code for several of these variables could lead to unphysical results. A good example is the choice of grid size. For the Freja applications to plasmas of quite low density, the real sheath size may easily extend outside the chosen simulation box edge. In that case, the sheath predicted by the code would be too

small, the ion currents underestimated and the magnitude of the charging level be overestimated. While this is easily detected, a more subtle effect is that even though the sheath boundary is well inside the simulation box, the boundary condition that the potential is zero one grid unit outside the simulation box could cause errors in the potential determination, and thereby in other parameters like the sheath location and in the prediction of barrier potentials.

While care has been taken to find and minimise such sources of error, using hints in the documentation and some highly appreciated input from other POLAR users including its creator/maintainer David Cooke, investigating all aspects of the POLAR code is a formidable task beyond the scope of this study. However, the results presented here are the results of quite extensive trial-and-error investigations and studies of parts of the code. In order for future tracing or ruling out of such errors, the simulation input files used in this study have been made available to the contractor.

We have seen that for at least one charging simulation (6a:1) the initial condition on potential was very important for the final outcome. This raises the question of the need to model the time history of spacecraft charging. Such a model could in principle be done with the existing POLAR 1.3.7 code, but would require a tremendous effort in practice: run a simulation, get potentials as initial conditions for next simulation, change parameters slightly (the driver of the process), run the simulation again and so on.

(d) *Code limitations*. POLAR has previously been used to simulate DMSP charging events, where higher plasma density was reported. The low plasma density in the Freja events makes sheath sizes large, which is a practical problem in a code using the fixed-grid-resolution strategy of POLAR, leading to unreasonable simulation times. The simulations reported in this study required simulation run times on the order of an hour (model A) to a few days (some model C runs), which may be considered a practical upper limit for many users. Nevertheless, simulations performed using NASCAP as well as POLAR for a –80 V charging event [Svensson, 1997] indicated that the sheath size limitation of POLAR cannot explain the discrepancy between simulation and observations, as NASCAP was no more successful in the case studied.

In addition, three of the five events studied here, and most of all observed Freja charging events, consider spacecraft potentials no lower than -50 V, while the driver for the development of POLAR and other charging codes is the study of higher levels of charging,

where potentially harmful effects in terms of arcing and discharging may set in if differential voltages appear. However, the biggest discrepancy between simulation and observations was seen to be in the highest charging level event. In the following section, we discuss some physical phenomena that possibly may need refined treatment in the code in order to model the Freja charging.

5.4 Suppression of secondary current and photoelectron current

In Section 5.2, it was seen that a direct best-effort approach to POLAR modelling of the Freja charging events did not reproduce the observed charging levels. Possible causes for this discrepancy related to spacecraft and plasma modelling and code handling was discussed above. Assuming no such errors exist, what physical effects could cause the observed discrepancy?

The main problem for getting the observed charging level in a POLAR simulation is that the secondary currents, and for the sunlit event 7 the photocurrent, must be suppressed. From studies of spacecraft in geostationary orbit, it is well known that one way of efficiently doing so is the build-up of barrier potentials related to differential charging [e.g. Purvis, 1983]. On Freja, such a scheme has its problems as the area of insulators is fairly small. On the other hand, the secondary yield of the carbon fibre elements (nozzle, TM antenna domes) are so low (compare Figure 7) that they possibly may charge differentially to very high voltages, and the Freja simulations indeed show some development of differential charging, as can be seen in Figure 21. It is therefore of interest to accurately model the suppression of secondaries and photoelectrons by barrier potentials.

The POLAR 1.3.7 algorithm for modelling this is rather simplistic. If the secondary current or photocurrent emitted by a surface is I_0 and the normal electric field E_n on the surface is such that the emitted electrons are attracted back to the surface, POLAR assumes that the actually escaping current is

$$I_{esc} = \frac{I_0}{1 - \Phi / U_0} \qquad (7)$$

where $\Phi = 2E_nD$, D is the grid cell size and U_0 = 1 V. Figure 35 shows a comparison between this model and the suppression resulting if assuming Boltzmann distributed electrons emitted along the surface normal into a purely normal electric field with potential barrier height equal to F. Temperatures 1.5 eV and 3 eV are used, approximately describing photoelectrons and secondary electrons, respectively. It is seen that for small barrier potentials, up to some 3 V, the current suppression of photoelectrons is more pronounced by POLAR than by the Boltzmann model. For secondaries, the corresponding limit value is about 9 V.

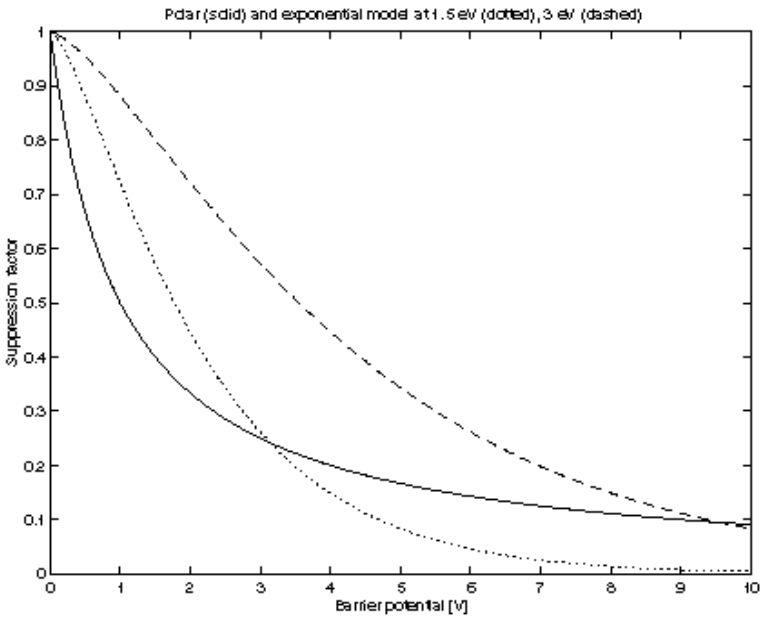

Figure 35. Comparison between the POLAR algorithm for suppression of photoelectrons and secondary electrons (solid curve) to a Boltzmann (dashed 3 eV, dotted 1.5 eV) with normal emission direction.

Neither the POLAR nor the Boltzmann algorithm takes higher-dimensional effects into account. For an infinite surface with a potential above it only depending of the coordinate along the surface normal, current limitation will be much severer than modelled above if electrons are emitted at all angles to the surface. On the other hand, the appearance of electric fields with a component perpendicular to the surface normal above the surface on a geometrically complex spacecraft will allow some particles escape above other surfaces than

those they were emitted from. Some particles will also hit the spacecraft at other surface elements that they were emitted from, a phenomenon called hopping. POLAR has a hopping model, unfortunately not supported in POLAR 1.3.7. This effect is therefore not included in the Freja simulations.

One may note that hopping and barrier formation are most effective in low density plasmas. In the charging situations previously studied with POLAR, densities have been higher and these effects therefore less unimportant [David Cooke, private communication]. It may therefore be fair to say that the POLAR algorithms are not operationally validated for the Freja environment. In order to treat hopping secondaries and barrier suppression correctly on a geometrically complex spacecraft, numerical integration of test particle orbits in the self-consistently determined potential distribution around the spacecraft would be desirable.

Another means of achieving suppression of emitted electrons from a spacecraft surface may be by the ambient magnetic field turning them back to the spacecraft. Laframboise [1988] has studied this effect for infinite planes and for various strengths of the normal electric field at the surface. To estimate the maximum importance of this effect, we have integrated Laframboise's fitted expression for the current suppression as a function of angle between surface normal and magnetic field over a sphere. The result should give some average value roughly applicable to a spherical spacecraft as long as its radius is much larger than the gyroradius (the infinite plane assumption). The lower normal electric field, the more pronounced the effect will be. As an upper limit of the importance of the effect, we assumed Freja to be a sphere of radius 0.7 m with a vacuum (Coulomb) electric field around it. The results are tabulated in Table 15, showing that the effect possibly may be of some importance for the low-level charging events but presumably not for the charging to hundreds of volts, particularly as the real electric field will be stronger than the vacuum field, thereby diminishing the importance of this effect. However, for low-charging or floating potential calculations its impact on the photoelectrons may be of interest.

Event	Iesc/I0
3	0.85
6a	0.90
6b	1.00
7	0.98
9	0.90

Table 15. Lower bound on ratio of escaping to emitted secondary current (or photocurrent in the case of event 7) calculated by averaging the result of Laframboise [1988] over the surface of a sphere of radius 0.7 m assuming Coulomb electric field at the surface.

5.5 Dynamic effects

In Section 2.5, we discussed the possibility of bifurcated equilibria and the time history of the charging process. We have seen that for at least one charging simulation (6a:1) the initial condition on potential was very important for the final outcome, and that such effects was found important also when running a variant of event 6b (Section 5.2.7). This raises the question of the need to model the time history of spacecraft charging. Such a model could in principle be done with the existing POLAR 1.3.7 code, but would require a tremendous effort in practice: run a simulation, get potentials as initial conditions for next simulation, change parameters slightly (the driver of the process), run the simulation again and so on.

6. CONCLUSION

6.1 Summary

A list of materials for the Freja satellite has been compiled. Material properties for these materials are known from laboratory experiments, except for some details like engine nozzles and TM antenna domes whose properties are not well known. Models of Freja at different resolution have been prepared, and five Freja events were studied in detail to provide information on the plasma environment in the charging events. The models of spacecraft and plasma were used as inputs to simulations using the POLAR code. It was found vital to compensate for the impact of the charging level of the spacecraft on the electron detectors when modelling the charging events for POLAR. The observed levels of charging were usually not reproduced by the code, although there were a few exceptions. For some events, the discrepancy is very large. Variations in hot and cold plasma density and temperature within reasonable limits cannot explain the discrepancy. It is possible that high energy electrons at pitch angles not covered by the detectors could be responsible: however, the inverted-V precipitation spectra that accompany the charging events are usually quite isotropic except for the loss cone. The Freja model is quite detailed and should not be a cause of the discrepancy, although erroneous material parameters for some of the applied surface material would be a problem if present. The numerical parameters for the code has been varied in numerous runs, and we do not believe unsuitable instructions to the code is a major error source, although this is hard to rule out using the POLAR documentation. Some physical processes not or insufficiently treated by POLAR may be the suppression of photocurrent and secondary electron current by potential barriers, hopping to other surfaces and, but presumably only for the lowest charging voltages, the magnetic field, and effects of the charging history of the spacecraft.

6.2 Suggestions for further studies

Some suggestions for further studies of the Freja events modelled here has been suggested in the sections above. As one of the possible error sources is the incomplete pitch-angle coverage of the electron detectors, some Freja events where this is more complete could be added. Another possibility is to use data from some other spacecraft, for which complete pitch angle coverage is always available.

A comparative study using NASCAP as well as POLAR should be useful. NASCAP was used initially in this work, and it was found that in order to reproduce observed charging levels in a test case, the density and temperature of the energetic electrons had to be increased by factors of 10 and 3, respectively, from the best-fit values [Svensson, 1996]. Later work was concentrated on POLAR as being the code developed for low-altitude auroral charging situations. However, it is possible that with the experiences gained during this work, as reproduced in this report, particularly the importance of correcting observed spectra for the spacecraft charging level, and with improved versions of NASCAP where more advanced particle spectra than superposed Maxwellians can be modelled, a renewed NASCAP effort could be fruitful. In particular, it could be interesting to run NASCAP and POLAR for cases where they both should be applicable. A NASCAP model of Freja could also include booms, to see the effect of adding and removing these.

6.3 Recommendations for code development

When POLAR arrived in the late eighties, it represented a major breakthrough in the study of charging effects in low Earth orbit in the auroral zone, by its ability to self-consistently model a spacecraft sheath, include wake effects and magnetisation, and its facilities for modelling auroral electron spectra. Applications of POLAR has mainly concerned objects large compared to the spacecraft size, which has shown that POLAR works well in this domain. The Freja situation, with the density so low that the Debye length is on the order of the spacecraft dimension, is something of a new application. If it is desirable to model this situation, we recommend that the Freja charging events are studied further as an input to code development. The Freja spacecraft and environment models used in this study are available for that purpose. In particular it should be useful to compare NASCAP and POLAR results for parameter domains where they both should provide useful values. These domains may not necessarily be exactly those observed.

For the low-density plasmas studied here, the size of the sheath and the boundary condition that the potential should be zero at the simulation box edges sometimes are problems, as they necessitate very large grids and thereby causes the calculation time to grow unpractically large. The possibility of employing some adaptive-grid algorithm at least outside the sheath should be considered, reducing the necessary grid resolution in this area and thus saving computational time without jeopardising the physical accuracy.

The POLAR tools for keeping track of electrostatic barrier formation and currents hopping between surface elements may be insufficient for the Freja case, where these features are of higher importance than in the denser plasmas studied in previous POLAR applications. This should be tested by comparison to NASCAP results and numerical studies of test particle motion in potential distributions around geometrically complicated objects before the importance of algorithm changes can be assessed.

For low-level charging events and floating-potential calculations, the inclusion of a magnetic limitation algorithm for the secondary current and photoelectron current could be of some importance. Such an algorithm should be fairly straightforward to implement, using the interpolation formula of Laframboise [1988]. This may possibly bring significant improvement for low level charging events (i.e., a few tenths of volts) and non-convex spacecraft geometries.

POLAR was developed in the eighties, as is clearly witnessed by the user interface. A modern graphical user interface would be a major improvement to the usability of the code.

ACKNOWLEDGEMENTS

Our sincere thanks first go to David Cooke of the US Air Force Research Laboratory, who graciously provided POLAR version 1.3.7 as well as useful comments and instructions for its use. The virtues of the simulation study are much thanks to him, while its vices are due to us. Thanks also to Peter Rathsman of the Swedish Space Corporation, who provided data on the Freja spacecraft surface materials, to Laila Andersson of the Kiruna Division of the Swedish Institute of Space Physics for providing the particle data, to Ulrika Svensson, who did an important initial study at ESTEC, and to Alain Hilgers of ESTEC for useful input and advice.

REFERENCES

Al´pert, Ya. L., Gurevich, A. V., and Pitaevskii, L. P., *Space physics with artificial satellites.* Consultants Bureau, Washington D.C., 1965.

Al´pert, Ya. L., *The near-Earth and interplanetary plasma, volume 2: Plasma flow, plasma waves and oscillations.* Cambridge University Press, Cambridge 1983.

André, Mats (editor): *The Freja Scientific Satellite*.. IRF Scientific Report 214, Swedish Institute of Space Physics, Kiruna 1993.

Boehm, M., G. Paschmann, J. Clemmons, H. Höfner, R. Frenzel, M. Ertl, G. Haerendel, P. Hill, H. Lauche, L. Eliasson and R. Lundin, The TESP electron spectrometer and correlator (F7) on Freja. *Space Sci. Rev., 70,* 509-540, 1994.

Cooke, D. L., M. Tautz and J. Lilley, Polar code simulation of DMSP satellite auroral charging. Paper presented at the AIAA meeting, Reno, Nevada, January 11, 1989.

Danilov, V., G. Drolshagen, V. M. Dvoryashin, A. M. Kramarenko, P. Pita Leira, V. S. Sokolov and Yu. V. Vasilyev, Numerical simulation of high-voltage charging at high altitudes: comparison of NASCAP and ECO-M. Presentation at *the 6th Spacecraft Charging Conference*, US Air Force Research Laboratory, November 2-6, 1998.

Eliasson, L., O. Norberg, R. Lundin, K. Lundin, S. Olsen, H. Borg, M. André, H. Koskinen, P. Riihelä, M. Boehm and B. Whalen, The Freja hot plasma experiment - instrument and first results. *Space Sci. Rev., 70,* 563-576, 1994.

Fontheim, E. G., K. Stasiewicz, M. O. Chandler, R. S. B Ong and T. Gombosi, Statistical study of precipitating electrons, *J. Geophys. Res., 87,* 3469-3480, 1982.

Frezet, M., E. J. Daly, J. P. Granger and J. Hamelin, Assessment of electrostatic charging of satellites in the geostationary environment. *ESA Journal, 13,* 89-116, 1989.

Hastings, D., A review of plasma interactions with spacecraft in low Earth orbit. *J. Geophys. Res., 100,* 14457-14483, 1991.

Hastings, D., and H. Garrett, *Spacecraft-environment interactions*. Cambridge University Press, Cambridge, 1996.

Hilgers, A., Statement of work, memorandum, estec/wma/94-273/ah, 1994.

Holback, B., S.-E. Jansson, L. Åhlén, G. Lundgren, L. Lyngdal, S. Powell, and A. Meyer, The Freja wave and plasma density experiment. *Space Sci. Rev., 70,* 577-592, 1994.

Katz, I., M. J. Mandell, G. Jongeward and M. S. Gussenhoven, The importance of accurate secondary electron yields in modelling spacecraft charging. *J. Geophys. Res.*, 91, 13739-13744, 1986.

Katz, I., G. A. Jongeward, V. A. Davis, M. J. Mandell, R. A. Kuharski, J. R. Lilley, Jr., W. J. Raitt, D. L. Cooke, R. B. Torbert, G. Larson and D. Rau, Structure of the bipolar plasma sheath generated by SPEAR-1. *J. Geophys. Res.*, 94, 1450-1458, 1989a.

Katz, I., J. R. Lilley, Jr., G. A. Jongeward, M. J. Mandell, and T. T. Luu, *Polar code validation*. Technical report GL-TR-89-0276, US Air Force Geophysics Laboratory, 1989b.

Krupnikov, K. K., V. N. Mileev, L. S. Novikov and G. V. Babkin, Mathematical modelling of high altitude spacecraft charging. In *Proceedings of the international conference on problems of spacecraft /environment interactions*, edited by G. Drolshagen, 167-175, Novosibirsk, Russia, 1992.

Lai, S. T., Theory and observation of triple-root jump in spacecraft charging. *J. Geophys. Res., 96,* 19269-19281, 1991.

Laframboise, J. G., Calculation of escape currents of electrons emitted from negatively charged spacecraft surfaces in a magnetic field. *J. Geophys. Res., 93,* 1933-1943, 1988.

Liley, John R., David L. Cooke, Gary A. Jongeward and Ira Katz, *POLAR User's Manual*. Technical report GL-TR-89-0307, Geophysics Laboratory, Air Force Systems Command, Hanscom AFB, Mass. 1989.

Lundin and Haerendel (editors), The Freja Science Mission, *Space Sci. Rev., 70,* 405-602, 1994.

Mandell, M. J., J. R. Lilley, Jr., and I. Katz, Computer modelling of current collection by the Charge-2 mother payload. In *Polar Code Validation*, technical report GL-TR-89-0276, US Air Force Geophysics Laboratory, 1989.

Medicus, G., Theory of electron collection of spherical probes. *J. Appl. Phys., 32,* 2512-2520, 1961.

Medicus, G., Spherical Langmuir probe in drifting and accelerated Maxwellian distributions. *J. Appl. Phys., 33,* 3094-3100, 1962.

Mott-Smith, H. M., and I. Langmuir, The theory of collectors in gaseous discharges, *Phys. Rev., 28,* 727-763, 1926.

Pedersen, A., C. A. Cattell, C.-G. Fälthammar, V. Formisiano, P.-A. Lindqvist, F. Mozer and R. Torbert, Quasistatic electric field measurements with spherical double probes on the GEOS and ISEE satellites. *Space Sci. Rev., 37,* 269-312, 1984.

Prokopenko, S. M. L., and J. G. Laframboise, High-voltage differential charging of geostationary spacecraft. *J. Geophys. Res., 85,* 4125-4131, 1980.

PUM, *Polar User's Manual*: see Liley et al. [1989].

Purvis, C. K., The role of potential barrier formation in spacecraft charging. In *Spacecraft/Plasma Interactions,* ESA SP-198, 115-126, European Space Agency, 1983.

Sheldahl, *Thermal control material & metalized films: part number listing and general specifications.* Sheldahl corporation, Northfield, MN, 1985.

Soop, M., Report on photoelectron calculations for the satellite GEOS . *Planet. Space Sci., 20,* 859-870, 1972.

Svensson, Ulrika, *Simulation of Spacecraft Charging in the Aurora: A Case Study*. ESTEC Working Paper 1943, ESTEC, Noordwijk 1997.

Tribble, Alan C., *The Space Environment.* Princeton University Press, Princeton, N.J., 1995.

Usui, H., H. Matsumoto and Y. Omura, Plasma response to high potential satellite in electrodynamic tether system. *J. Geophys. Res., 98,* 1531-1544, 1993.

Wahlund, J.-E., L. Wedin, A. I. Eriksson, B. Holback and L. Andersson, Analysis of Freja charging events: Charging events identification and case study of a subset of them. WP 130 technical note (SPEE-WP130-TN). Published as *IRF Scientific Report 251*, Swedish Institute of Space Physics, Kiruna, 1998a.

Wahlund, J.-E., L. Wedin, T. Carozzi, A. I. Eriksson, B. Holback, L. Andersson and H. Laakso, Analysis of Freja charging events: Statistical occurrence of charging events. WP 130 technical note (SPEE-WP130-TN). Published as *IRF Scientific Report 253*, Swedish Institute of Space Physics, Kiruna, 1998b.

WP110: See Wahlund et al., 1998a.

WP130: See Wahlund et al., 1998b.